STARS

University of Central Florida
STARS

Electronic Theses and Dissertations, 2004-2019

2017

Noise, Stability, and Linewidth Performance of 10-GHz Optical Frequency Combs Generated from the Nested Cavity Architecture

Kristina Bagnell
University of Central Florida

 Part of the Electromagnetics and Photonics Commons, and the Optics Commons
Find similar works at: https://stars.library.ucf.edu/etd
University of Central Florida Libraries http://library.ucf.edu

This Doctoral Dissertation (Open Access) is brought to you for free and open access by STARS. It has been accepted for inclusion in Electronic Theses and Dissertations, 2004-2019 by an authorized administrator of STARS. For more information, please contact STARS@ucf.edu.

STARS Citation
Bagnell, Kristina, "Noise, Stability, and Linewidth Performance of 10-GHz Optical Frequency Combs Generated from the Nested Cavity Architecture" (2017). *Electronic Theses and Dissertations, 2004-2019*. 5579.
https://stars.library.ucf.edu/etd/5579

NOISE, STABILITY, AND LINEWIDTH PERFORMANCE OF 10-GHZ OPTICAL FREQUENCY COMBS GENERATED FROM THE NESTED CAVITY ARCHITECTURE

by

KRISTINA M. BAGNELL
B.S. University of Florida, 2011
M.S. University of Central Florida, 2014

A dissertation submitted in partial fulfillment of the requirements
for the degree of Doctor of Philosophy
in CREOL, The College of Optics and Photonics
at the University of Central Florida
Orlando, Florida

Summer Term
2017

Major Professor: Peter J. Delfyett, Jr.

© 2017 Kristina M. Bagnell

ABSTRACT

Optical frequency combs with wide mode spacing and low timing jitter are relied upon for both time domain and frequency domain applications. It has been previously demonstrated that surrounding a low-Q semiconductor laser chip with a long external fiber cavity and inserting a high finesse Fabry–Pérot etalon into this cavity can produce a mode-locked laser with the desired high repetition rate and narrow optical mode linewidths which are of benefit to applications like photonic analog-to-digital conversion and astronomical spectrograph calibration. With this nested cavity architecture, the quality factor of the resonator is effectively determined by the product of the individual quality factors of the long fiber cavity and the short etalon cavity.

Passive cavity Q and intracavity power both influence mode-locked laser mode linewidth, optical frequency stability, and the phase noise of the photodetected output. The nested cavity architecture has been demonstrated at 10-GHz mode spacing a few times with increasing etalon finesse and once with a high saturation power semiconductor gain medium to increase intracavity power. No one system has been fully characterized for long term optical frequency stability, phase noise and timing jitter, and optical mode linewidth. As a result, the trade-offs involved with advancing any one element (e.g. increasing cavity Q by adding fiber length and maintaining a broad spectral region of low dispersion for broad-bandwidth operation) have not been fully examined. In this work, three cavity elements are identified for study to influence cavity Q, effective noise spur suppression, and intracavity power, and the trade-offs of pushing those parameters to new limits are experimentally demonstrated. In the process, we also demonstrate nested cavity systems with fractional frequency instability on the order of 10^{-13}, timing jitter as low as 20 fs, and Hz-level linewidths.

For my husband, Tony, who is truly the best around.

ACKNOWLEDGMENTS

First and foremost, I would like express my gratitude to my advisor, Professor Peter Delfyett for his guidance and inspiration throughout my graduate school career. I would also like to state how privileged I feel to have worked with my colleagues in the Ultrafast Photonics group from whom I learned so much during my time in the group. They are Dr. Umar Piracha, Dr. Nazanin Hoghooghi, Dr. Josue Davila-Rodriguez, Dr. Charles Williams, Dr. Dat Nguyen, Dr. Marcus Bagnell, Dr. Sharad Bhooplapur, Dr. Abhijeet Ardey, Dr. Edris Sarailou, Dr. Anthony Klee, Abdullah Zaman, Michael Plascak, and Ricardo Bustos Ramirez.

TABLE OF CONTENTS

ABSTRACT iii

ACKNOWLEDGMENTS v

TABLE OF CONTENTS vi

LIST OF FIGURES viii

LIST OF TABLES xiv

LIST OF ACRONYMS/ABBREVIATIONS xv

CHAPTER 1: MOTIVATION 1

CHAPTER 2: BACKGROUND AND ARCHITECTURE 5

2.1 Semiconductor gain with external fiber cavity 6

2.2 Supermode suppression 10

2.3 Length stabilization 11

2.4 Dispersion compensation 14

2.5 Summary of the Nested Cavity Architecture 15

2.6 Previous Work 16

CHAPTER 3: OPTICAL AND RF PERFORMANCE ASSOCIATED WITH CAVITY LENGTH AND INTRACAVITY POWER 17

3.1 Optical performance 17

3.1.1 Linewidth 17

3.1.2 Optical combline stability 20

3.2 RF performance: residual phase noise 22

3.3 Proposed systems 25

CHAPTER 4: TRADE-OFFS ASSOCIATED WITH LENGTH, GAIN SATURATION, AND FPE FINESSE 30

4.1 Cavity length and operating bandwidth 30

4.2 Gain and saturation power 31

4.3 Length and free-running stability 32

CHAPTER 5: NOTABLE RESULTS 34

5.1 System Performance 34

5.1.1 System 1: SOA, short cavity, 10000 finesse FPE 34

5.1.2 System 2: SOA, long cavity, 10000 finesse FPE 37

5.1.3 System 3: SCOWA, short cavity, 10000 finesse FPE 39

5.1.4 System 4: SCOWA, long cavity, 10000 finesse FPE 43

5.1.5 System 5: SCOWA, short cavity, 1000 finesse FPE 45

5.2 Discussion 47

5.2.1 Phase Noise of Photodetected Output 47

5.2.2 Long term Optical Frequency Stability 48

5.2.3 Optical Mode Linewidth 49

CHAPTER 6: SUMMARY AND OUTLOOK 55

REFERENCES 57

LIST OF FIGURES

Figure 1 Generic OFC's spectral (top) and temporal (bottom) characteristics..... 1

Figure 2 Fundamental mode-locking in the frequency domain (a), time domain (b), and implementation as a ring laser cavity (c) 6

Figure 3 Passive cavity resonances: Top: 10 GHz chip (refractive index = 3.3, facet reflectivity 0.3); Bottom: 10 m fiber cavity (refractive index = 1.5, ring cavity with 10% output coupling). The width of the passive resonances of the long cavity are narrower by about four orders of magnitude. 7

Figure 4 Harmonic mode-locking, two interpretations. Center: harmonically mode-locked spectrum and pulse train; left: overlapped high repetition rate pulse trains and interleaved broadly-spaced frequency supermodes; right: interleaved low repetition rate pulse trains and overlapped narrowly-spaced comb spectra..... 9

Figure 5 Phase noise measurement of a harmonically mode-locked laser with no effort made to suppress supermodes. The mode-locked laser has a cavity length of 351 m, corresponding to a fundamental cavity frequency of 570 kHz. A semiconductor optical amplifier is used for the laser gain medium and the repetition rate is 10.24 GHz. Discontinuities are an artifact of stitching between frequency bands with measurements using different resolution bandwidth..... 10

Figure 6 Supermode suppression via FPE to match a harmonic mode-locking rate of n=3. Left: FPE transmission spectrum; right: implementation in a ring laser cavity (FPE length not shown to scale with rest of cavity) 11

Figure 7 FPE magnitude (left) and phase (right) response upon reflection as a function of detuning of incident laser frequency from the passband for FPEs of finesse 2 (blue) and 30 (red)..... 13

Figure 8 Conventional PDH CW laser frequency stabilization setup..... 13

Figure 9 Multi-combline PDH setup implementation in a ring laser cavity (in green shading)... 14
Figure 10 Full nested cavity architecture: ISO (Isolator), PC (polarization controller), FPE (Fabry–Pérot Etalon), PBS (polarization beam splitter), OC (optical coupler), FS (piezoelectric fiber phase shifter), VOD (free-space variable optical delay), IM (Mach-Zehnder intensity modulator), SMF (standard single mode fiber), DCF (normal dispersion fiber), PM (phase modulator), CIRC (circulator), PD (photodetector), DBM (double balanced mixer), PS (RF phase shifter), LPF (low pass filter)..... 16
Figure 11 (a) heterodyne beat measurement setup for linewidth measurement. RT-RFSA: Real-Time RF Spectrum Analyzer; (b) linewidth measurement data for a short cavity (red) and a long cavity (black); (c) close-in view of the same data as (b) with Lorentzian fits in dashed lines. Asymmetry in data traces is thought to be a result of beatnote movement during data capture and the operation near the resolution limit of the reference source used in this measurement (30 Hz). 19
Figure 12 (a) Allan deviation: a frequency counter counts the number of zero crossing events during consecutive time windows of length τ and computes the average frequency during each bin; (b) Computation of the Allan deviation gives deviation characteristics at different timescales; (c) measurement setup..... 21
Figure 13 (a) Residual phase noise setup (b) illustrated example of a typical single-sideband phase noise measurement from a harmonically mode-locked laser..... 24
Figure 14 Residual phase noise measurements for two systems of different length, showing the decrease in white noise corner frequency and in supermode spur offset frequency. The short cavity's phase noise performance (black) was also shown in Figure 5 to illustrate supermode noise spurs in harmonic mode-locking..... 25

Figure 15 White noise corner frequency (black) and linewidth (red) dependence on cavity length and square of cavity length, respectively. The four new data points agree with the predictions made about the relation of laser linewidth and passive resonance width to cavity length in CHAPTER 2:. Data in “Previous Results” shaded box taken from Yilmaz et al [15]..... 26
Figure 16 (a) Gain saturation curves for a commercially available SOA device and for the SCOWA device driven at their respective maximum rated currents (b) SCOWA device cross-section showing low optical mode confinement and overlap with the active gain region [53] 27
Figure 17 Optical and RF characterization data for System 1 (SOA, short cavity, 10k finesse FPE). (a) Optical spectrum; (a, inset) Hi-res optical spectrum; (b) photodetected RF spectrum; (c) sampling scope trace of photodetected compressed pulses; (d) autocorrelation for uncompressed (black), compressed (blue) and transform-limited (red) pulses 35
Figure 18 (a) Heterodyne beat with a 100 Hz reference CW laser (black), Lorentzian function with 1.3 kHz FWHM (red). The center frequency of the heterodyne beatnote was 4 GHz (b) Allan deviation data for a heterodyne beat with a cavity-stabilized CW laser, normalized to the optical frequency of 193.4 THz. The center frequency of the heterodyne beatnote was 4.6 GHz. 36
Figure 19 Phase noise data for System 1 (SOA, 10k finesse FPE, short cavity length). Single sideband phase noise (left axis) and integrated timing jitter (right axis) for the photodetected pulse train (red) and for the measurement floor (black). 36
Figure 20 Optical and RF characterization data for System 2 (SOA, Long cavity, 10k finesse FPE). (a) Optical spectrum; (a, inset) Hi-res optical spectrum; (b) photodetected RF spectrum; (c) sampling scope trace of photodetected compressed pulses; (d) autocorrelation for uncompressed (black), compressed (blue) and transform-limited (red) pulses 38

Figure 21 (a) heterodyne beat between a combline from System 2 and a 100-Hz CW reference laser. A 150 Hz Lorentzian function is shown in red for visual aid; (b) Allan deviation measurement of a heterodyne beat with a cavity-stabilized CW laser, normalized to the optical frequency of 193.4 THz 39
Figure 22 Optical and RF characterization data for System 3 (SCOWA, Short cavity, 10k finesse FPE). (a) Optical spectrum; (a, inset) Hi-res optical spectrum; (b) photodetected RF spectrum; (c) sampling scope trace of photodetected compressed pulses; (d) autocorrelation for uncompressed (black), compressed (blue) and transform-limited (red) pulses 40
Figure 23 Phase noise data for System 3 (SCOWA, short cavity, 10k finesse): Single sideband residual phase noise (left axis) and integrated timing jitter (right axis) for the photodetected pulse train (red) and the measurement setup noise floor (black) 41
Figure 24 (a) Heterodyne beat between a combline from System 3 and a 100-Hz CW reference laser. A 125 Hz Lorentzian function with an added noise floor is shown in red for visual aid; (b) Allan deviation measurement of a heterodyne beat with a cavity-stabilized CW laser, normalized to the optical frequency of 193.4 THz 42
Figure 25 Optical and RF characterization data for System 4 (SCOWA, Long cavity, 10k finesse FPE). (a) Optical spectrum; (a, inset) Hi-res optical spectrum; (b) photodetected RF spectrum; (c) sampling scope trace of photodetected compressed pulses; (d) autocorrelation for uncompressed (black), compressed (blue) and transform-limited (red) pulses 44
Figure 26 Linewidth and long term stability data for System 4 (SCOWA, long cavity, 10k finesse): (a) heterodyne beat with a 100-Hz reference CW laser. The beatnote center frequency was ~4 GHz. The measurement limit of a 100-Hz Lorentzian function with an added noise floor of -58 dBc/Hz

(red) is shown for visual aid; (b) Allan deviation measurement of a heterodyne beat with a cavity-stabilized CW laser. 45

Figure 27 (a) heterodyne beat between a combline from System 5 and a 100-Hz CW reference laser. A 300 Hz Lorentzian function with an appropriate noise floor level is shown in red for visual aid; (b) Allan deviation measurements of a heterodyne beat with a cavity-stabilized CW laser, normalized to the optical frequency of 193.4 THz for both System 3 (black) and System 5 (red) 46

Figure 28 Single sideband residual phase noise measurement for Systems 1 (green) and 3 (red), with associated measurement noise floors (muted green, muted red, respectively). 47

Figure 29 Allan deviation data for all configurations using an FPE of finesse 10^4. Long cavities (red) short cavities (black) SCOWA (square symbol) and SOA (triangle symbol) 49

Figure 30 Selected comparisons in linewidth performance vs. passive cavity resonance width of nested cavity systems. Gray shaded region of each plot represents range of curves with output powers lying between 2 and 12 mW. Dotted lines are the specific linewidth curve determined by the power of the system under study (a) SOA, 10^4 finesse systems with short length (red) and long length (green); (b) Short, 10^4 finesse systems with SOA gain medium (red) and SCOWA gain medium (blue); (c) Short SCOWA systems with 10^3 finesse FPE (pink) and 10^4 finesse FPE (blue); (d) SCOWA, 10^4 finesse FPE systems with short length (blue), and the expected linewidth performance for long cavity length (light blue). 53

Figure 31 Compiled and annotated linewidth results. Gray shaded region: range of linewidth performance curves for systems with output powers between 2 and 12 mW. Agreeing with theory, linewidth decreases with longer cavity length, and increases with increased cavity losses. Also

agreeing with theory, the relationship between the linewidth performance short and long configurations is the same for SCOWA-based and SOA-based systems 54

LIST OF TABLES

Table 1 Enumeration of the proposed systems to measure 28

Table 2 Loss budget of cavity elements (excluding gain medium) 32

Table 3 Comparison of optical mode linewidths between the 5 systems (FPE Finesse = 10^4 unless otherwise indicated) 50

Table 4 Additional relevant parameters for linewidth comparison. 51

LIST OF ACRONYMS/ABBREVIATIONS

AOM – Acousto-Optic Modulator

CW – Continuous Wave

DCF – Dispersion Compensating Fiber

DUT – Device Under Test

FPE – Fabry–Pérot Etalon

FS – Fiber Stretcher

FSR – Free Spectral Range

IM – Intensity Modulator

ISO - Isolator

LPF – Low-Pass Filter

OC – Output Coupler

OFC – Optical Frequency Comb

PBS – Polarization Beam Splitter

PC – Polarization Controller

PD - Photodetector

PDH - Pound Drever Hall

PM – Phase Modulator

PS – Phase Shifter

SG – Signal Generator

SOA – Semiconductor Optical Amplifier

SCOWA – Slab-Coupled Optical Waveguide Amplifier

VOD – Variable Optical Delay

CHAPTER 1: MOTIVATION

Optical frequency combs (OFCs) with multigigahertz spacing and excellent timing jitter are relied upon for applications in both the frequency and the time domain. In the time domain, an OFC produces a periodic signal with repetition period $T_{rep.}$ The electric field carrier may lag or lead the intensity envelope, leading to a carrier envelope phase slippage (ϕ_{ceo}) between consecutive periods. In the frequency domain, the OFC comprises a set of equally spaced optical modes which have a fixed phase relationship to one another. Their frequency spacing is the repetition rate f_{rep}, which is equal to the inverse of the repetition period, and extending these optical modes down to DC results in the lowest mode having some offset from zero frequency related to the carrier envelope phase slippage called the carrier envelope offset frequency (f_{ceo}). Knowledge of these two parameters can define the absolute frequency of any combline in the OFC [1].

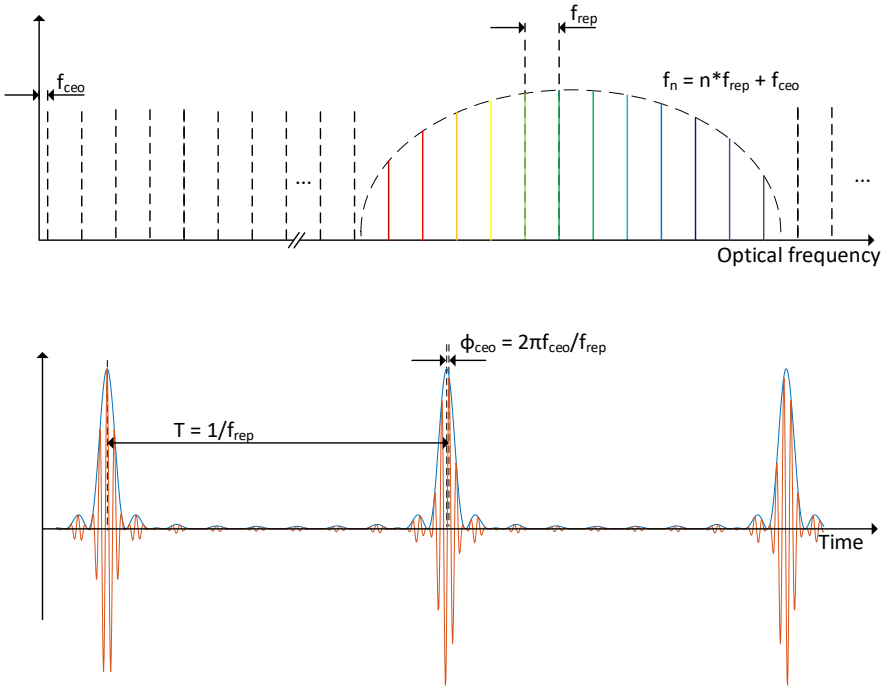

Figure 1 Generic OFC's spectral (top) and temporal (bottom) characteristics

A high repetition rate pulse train with low timing jitter enables accurate and precise photonic microwave generation [2], photonic analog-to-digital conversion [3, 4], and laser ranging and radar [5-7]. Piracha, et al. demonstrated laser radar capabilities of submillimeter range measurements of 15km and Doppler velocity measurements of a target moving at 92 m/s (330 km/h) using a 20 MHz pulse train.

Other applications like dual frequency comb spectroscopy [8] and astronomical spectrograph calibration [9] benefit from combs with ultra-narrow mode linewidth and from excellent long-term offset frequency stability. Long-term stability also makes the optical frequency comb a good candidate for optical referencing [10].

Harmonically mode-locked external-cavity semiconductor lasers have been demonstrated to have excellent timing jitter [11]. Their timing noise performance is improved when the supermode noise spurs which occur at harmonics of the fundamental cavity frequency are suppressed [12]. The method for supermode suppression in the latter work is the insertion of a short, high-finesse Fabry–Pérot Etalon (FPE) with free spectral range (FSR) matching the laser repetition rate. It serves as a periodic optical filter to select one supermode for oscillation. This architecture is most completely described as a harmonically mode-locked semiconductor-based external-cavity laser with intracavity etalon, but for the remainder of the document, the term "nested cavity architecture" may be used for brevity's sake.

Over time, this nested cavity architecture has been advanced by improving the specification of one intracavity element to improve a related performance metric. For example, intracavity power was increased by replacing the original gain element with a high saturation power one in order to drive the shot noise floor of the phase noise measurement down [13, 14]. In another study,

cavity length was increased to achieve a narrower optical mode linewidth and lower white noise corner frequency in the phase noise measurement [15].

So far, no one implementation of this system architecture has had the full suite of measurements performed, including linewidth, pulse width, phase noise, and long-term frequency stability. As a result, the tradeoff associated with improving one performance aspect, possibly at the expense of another one, has not been fully analyzed.

There are known interplays which will be presented in Chapter 4. One example is that optical mode linewidth varies with the inverse of both cavity length and intracavity power. So one might expect that increasing the length of the external fiber cavity would yield a lower mode linewidth. However, increasing the fiber cavity length adds dispersion, which starts to limit the mode-locking bandwidth, resulting in longer pulse. If a short pulse is still desired, adding dispersion compensation can flatten the overall cavity dispersion and broaden the bandwidth again to maintain the short pulse of the short cavity. But dispersion compensation adds loss to the cavity, which decreases the intracavity power, and, with it, the optical mode linewidth, working against the original goal.

This work builds on past research to attempt to improve optical and RF performance (namely linewidth and phase noise) of this laser system by increasing cavity length and gain saturation power. At the same time, however, we propose taking a step back to fully examine the trade-offs associated with improving these system elements. This architecture is by its nature reconfigurable to suit the requirements of its application, so we present a thoughtful parametric study of how performance suffers or is improved by a change to the system.

The remainder of this dissertation is split into three main parts to support the argument for this work. CHAPTER 2: is devoted to background knowledge. The system architecture is built

from the ground up while introducing the key concepts which have led to the decisions made about the progression of the system. CHAPTER 3: builds on the background introduced in Chapter 2 to introduce the system performance metrics of interest (phase noise, optical linewidth, and frequency stability) and techniques to measure these quantities. Saturation power and passive cavity resonance width are identified as two cavity parameters which play a role in the output performance metrics to be studied. Three cavity elements which largely determine those cavity parameters (cavity length, FPE finesse, and gain saturation power) are selected for study and a case for a methodical series of measurements to examine their interplay is made. CHAPTER 4: discusses predicted and already-observed trade-offs and diminishing returns associated with incrementing the cavity elements identified in Chapter 3. CHAPTER 5: presents the characterization of selected systems individually first, and second in relation to each other to see trends in performance as cavity elements are incremented.

CHAPTER 2: BACKGROUND AND ARCHITECTURE

An optical frequency comb can be generated from various sources including cascaded electro-optic modulators, microring resonators, and mode-locked lasers [16-21]. The work presented here focuses on a mode-locked laser system. Mode-locked lasers rely on some element within the laser cavity to produce the fixed phase correlation across the laser's output spectrum. Mode-locking can be either "passive", relying on a nonlinear process like Kerr lensing [22] or saturable absorption [23], "active", relying on actively varying the loss, gain, or phase of a cavity at a fixed frequency from an external source [24, 25], or some combination of passive and active termed "hybrid" [26]. The system under study is actively mode-locked via loss modulation.

Figure 2 illustrates the concept of fundamental active mode-locking via loss modulation, when the mode-locking rate is equal to the fundamental cavity frequency. In the frequency domain, an oscillating axial mode experiences modulation with sidebands exactly coinciding with the nearest neighboring axial modes. Since all oscillating modes see this modulation rate, energy is shared across the spectrum and the fixed phase relationship is developed. In the time domain, gain is constant with time and the intensity modulator (IM) varies the loss of the cavity with a period equal to the cavity round trip time (T_{rt}). Unlike a pulse generation technique like Q-switching, at steady state operation, the pulse is the same after many round trips.

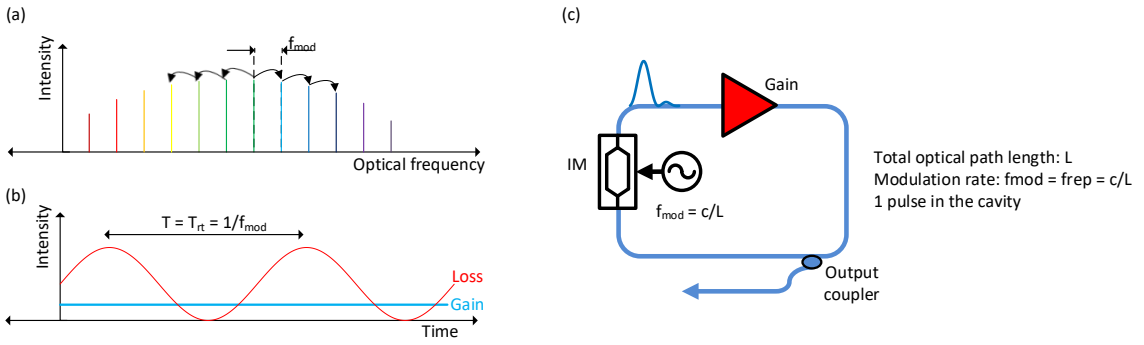

Figure 2 Fundamental mode-locking in the frequency domain (a), time domain (b), and implementation as a ring laser cavity (c)

The laser architecture presented in this dissertation proposal is based upon research and development over the past decade [12, 14, 27-30]. In the following sections, we will build up the system before presenting the complete architecture in Section 2.5.

2.1 Semiconductor gain with external fiber cavity

A mode-locked frequency comb can be produced from several different choices of gain medium. Semiconductor gain is chosen here for a few reasons. Semiconductor gain media have the potential for bandgap engineering over a broad range of wavelengths that are of interest for some of the applications discussed in CHAPTER 1: [31]. In addition, semiconductor diode lasers are cost-effective, electrically-pumped, and robust.

Semiconductor optical amplifiers (SOAs) are small and compact, but often have low finesse. The passive cavity resonances are broad in comparison to the chip FSR. In order to achieve narrow linewidth, an external fiber ring cavity is added around the SOA. Passive resonator free spectral range (f_{fsr}) and Finesse (F) can be calculated as follows:

$$f_{fsr} = {}^{c}/_{nL}$$

$$F = {}^{\pi\sqrt{R_1R_2}}/_{(1-R_1R_2)} = {}^{f_{fsr}}/_{\Delta f_{LW}}$$

Here, nL is the optical path length of the cavity, R_1 and R_2 are the mirror reflectivities for a linear cavity, and Δf_{LW} is the width of a resonance. All other things equal, a long cavity's passive modes have narrower axial mode linewidth compared to the short cavity. Figure 3 shows the passive resonances of a chip laser (top, R1=R2 = 0.3, FSR = 10 GHz) and a fiber cavity of length 10 m (bottom, n=1.5, 10% output coupling, FSR = 20 MHz).

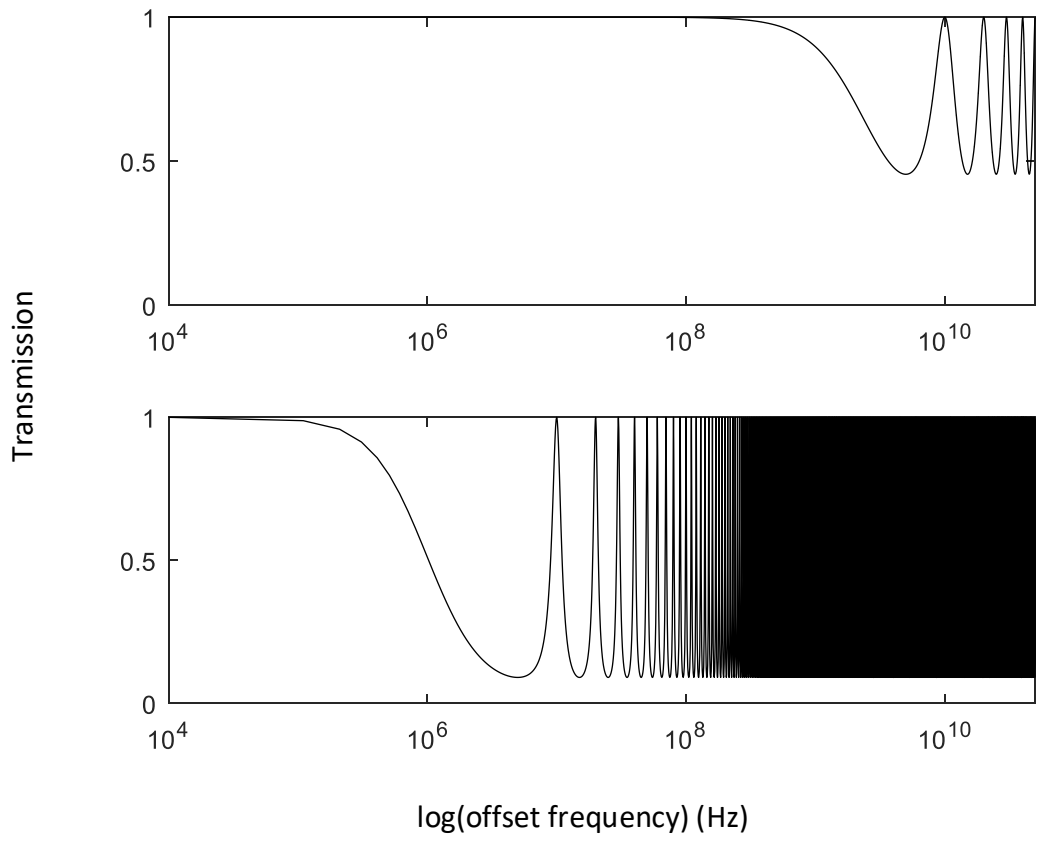

Figure 3 Passive cavity resonances: Top: 10 GHz chip (refractive index = 3.3, facet reflectivity 0.3); Bottom: 10 m fiber cavity (refractive index = 1.5, ring cavity with 10% output coupling). The width of the passive resonances of the long cavity are narrower by about four orders of magnitude.

The external fiber cavity added in Section 2.1 has a fundamental cavity frequency three orders of magnitude lower than the required ~10s of gigahertz. To achieve this high repetition rate, the loss is modulated at a harmonic of the fundamental mode spacing. For the example shown in

Figure 3, operation at 10 GHz would be operating at the 500th harmonic. Harmonic mode-locking has the advantage of achieving both the high repetition rate characteristic of a short laser cavity and the narrow mode linewidth characteristic of a long one.

Harmonically mode-locking at the Nth harmonic of the fundamental cavity frequency generates N equally spaced pulses existing in the laser cavity simultaneously[32]. This concept is illustrated on the right side of Figure 4. These three low repetition rate pulse trains are interleaved in time, and their closely spaced spectral content are superimposed, with some phase difference due to their separation in time. Another way to view harmonic mode-locking is the converse: interleaved broadly-spaced frequency modesets and superpositions of high repetition rate pulse trains. In this view, an oscillating laser axial mode experiences intensity modulation and its sideband coincides with the laser axial mode at an offset of N times the fundamental cavity frequency. Since those axial modes are also seeing modulation, that whole modeset has a fixed phase relationship as is dictated by mode-locking. This one widely spaced frequency modeset is referred to as a supermode. For harmonic mode-locking at N times the fundamental frequency, there are N interleaved supermodes existing in the cavity. In the time domain, these interleaved supermodes are a superposition of high repetition rate pulse trains. This is illustrated on the left side of Figure 4 with a harmonic mode-locking rate of N=3.

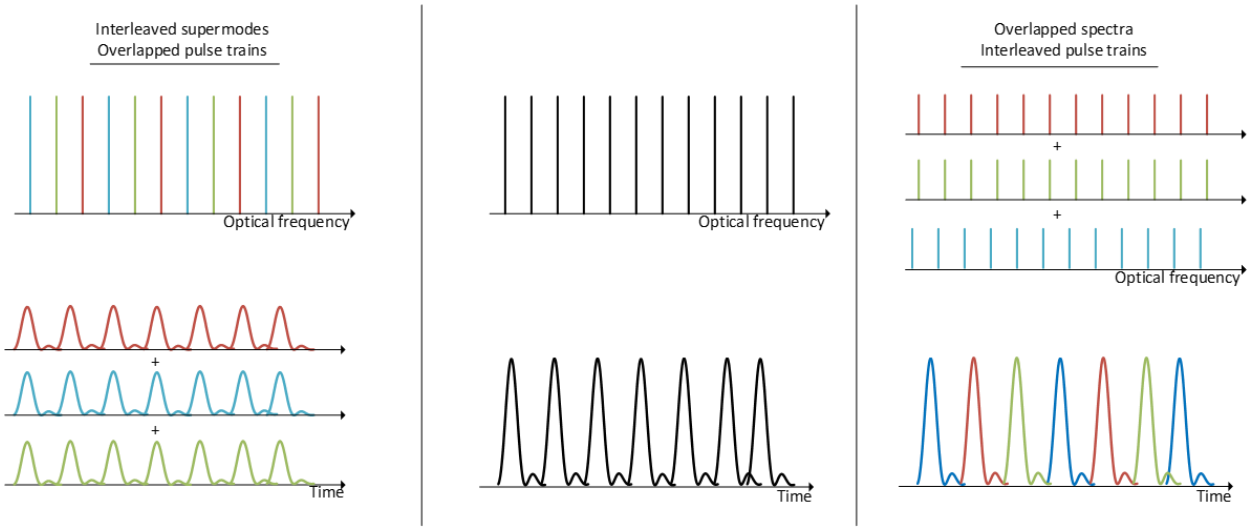

Figure 4 Harmonic mode-locking, two interpretations. Center: harmonically mode-locked spectrum and pulse train; left: overlapped high repetition rate pulse trains and interleaved broadly-spaced frequency supermodes; right: interleaved low repetition rate pulse trains and overlapped narrowly-spaced comb spectra.

What is not evident in Figure 4 is the noise that results from these supermodes being uncorrelated with each other. While each supermode has a fixed phase relationship across its spectrum, there is no fixed phase relationship between supermodes. The measurable effect is noise in timing and amplitude from pulse to pulse. This noise is manifested in the phase noise measurement of the photodetected pulse train as spurs at offset frequencies corresponding to harmonics of the fundamental cavity frequency. Figure 5 shows a phase noise measurement of the photodetected pulse train output from a mode-locked laser cavity where there has been no effort to suppress the supermode noise spurs [33]. Timing jitter can be calculated by integrating the phase noise from close to the carrier out to the Nyquist frequency (see Section 3.2). For the system shown in Figure 5, each supermode spur is contributing nearly 1 fs of timing jitter. Suppressing the spurs would be advantageous for applications requiring more precise timing.

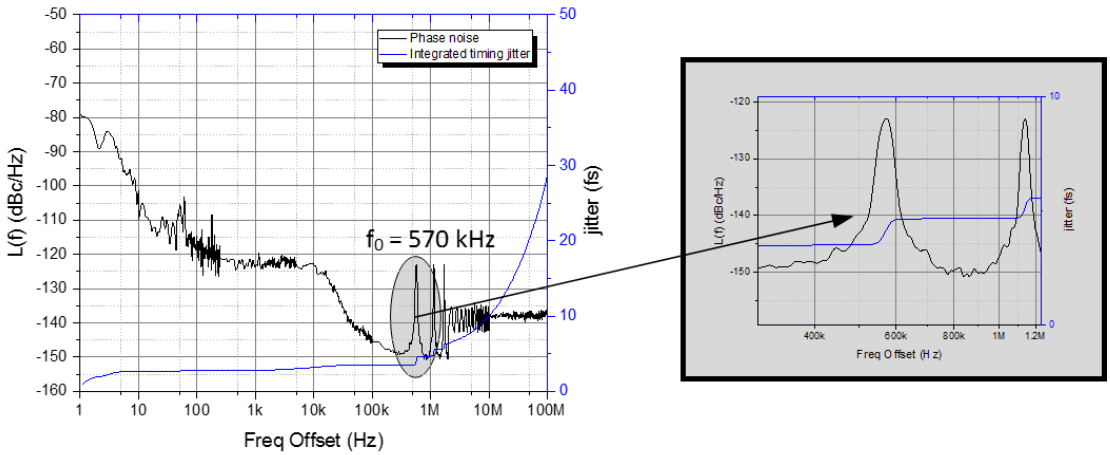

Figure 5 Phase noise measurement of a harmonically mode-locked laser with no effort made to suppress supermodes. The mode-locked laser has a cavity length of 351 m, corresponding to a fundamental cavity frequency of 570 kHz. A semiconductor optical amplifier is used for the laser gain medium and the repetition rate is 10.24 GHz. Discontinuities are an artifact of stitching between frequency bands with measurements using different resolution bandwidth.

2.2 Supermode suppression

There are a few methods of supermode suppression including CW laser injection-locking [34, 35] and nonlinear polarization rotation [36]. Another solution, which provides better supermode suppression, is to insert a periodic optical filter such as an FPE with a free spectral range matching the harmonic mode-locking rate to pass just one supermode and provide sufficient loss for all other cavity modes in order to prevent their oscillation. This nested cavity technique has been demonstrated successfully for several lasers and has been shown to suppress supermodes to below the shot noise floor on a single-sideband phase noise measurement, thus also removing measurable timing jitter associated with those supermodes [12, 14, 27-30]. Figure 6 illustrates supermode suppression in the optical domain and shows an example implementation in a ring laser cavity with a harmonic mode-locking ratio of n= 3. The FPE passbands coincide with just one supermode in the cavity. For a given FSR the finesse of the FPE indicates how frequency-selective

the FPE is, and determines how well the nearest supermode is suppressed. As the length of the external fiber cavity is increased, a higher finesse FPE is required to effectively suppress the neighboring supermode.

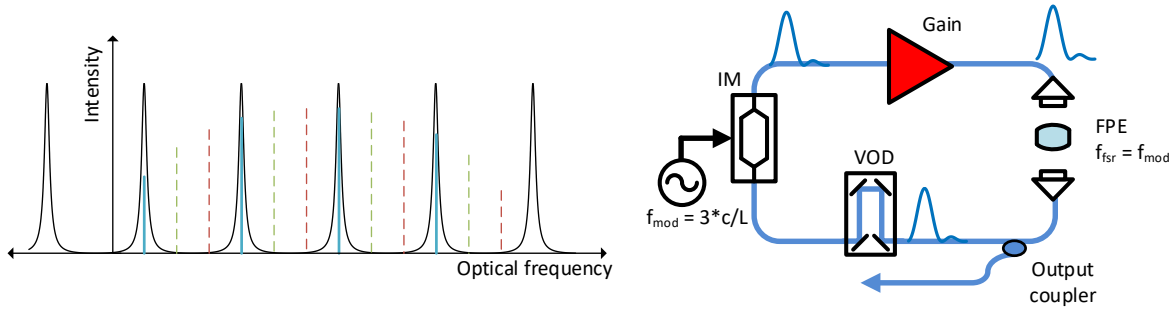

Figure 6 Supermode suppression via FPE to match a harmonic mode-locking rate of n=3. Left: FPE transmission spectrum; right: implementation in a ring laser cavity (FPE length not shown to scale with rest of cavity)

To closely match the length of the external cavity with a harmonic of that of the nested FPE, a free-space variable optical delay (VOD) is also convenient to add to the cavity.

2.3 Length stabilization

A high finesse etalon achieves supermode suppression, but creates the requirement for laser stabilization. For example, given an FPE FSR of 10 GHz, and a short external laser fiber cavity length of 10 m (f_0 = 20 MHz, operating at 500th harmonic), a change in fiber length of just 1 μm can shift the supermodes of the fiber cavity enough so that a particular FPE resonance passing an axial mode within the mth supermode instead coincides with one in the (m+1)th supermode. This effect only gets more dramatic with increasing length. A change in fiber length of 1 μm could easily result from a small change in ambient temperature or from an acoustic disturbance [37]. For an equivalent etalon-less cavity, with a slight change in cavity length, we'd see a shift in optical frequency with some noise introduced due to not having a modelocking rate closely matched to a

harmonic of the laser fundamental frequency. With the etalon in place, however, the shift in frequency can cause destabilization of mode-locking, or even the complete cessation of laser operation at the desired wavelength.

The well-known Pound-Drever-Hall (PDH) stabilization technique is slightly modified for use here [12, 38, 39]. In conventional PDH laser frequency stabilization, the CW laser to be frequency-stabilized is phase modulated and reflected off one mirror of a FPE. When the reflected light is photodetected and mixed with the drive signal to the phase modulator, an error signal is obtained. Because of the odd phase response of a FPE upon reflection (see Figure 7) and because the lower phase modulation sideband is of the opposite phase as the main tone and upper sideband (i.e., the photodetected signal is null without the odd FPE phase transfer function), the obtained error signal has high SNR and discriminates whether the CW laser tone is lower or higher in frequency than the etalon passband. An acousto-optic modulator is used as the feedback point to correct the laser frequency. A PDH stabilization setup is shown in Figure 8 along with sample error signals. One can use a phase modulation frequency on the order of the FSR to perform a precise FSR measurement with precision of 1 part in 10^6 [40], or a low phase modulation frequency well within the stopband of the etalon transfer function so that transmitted light has well-suppressed sidebands.

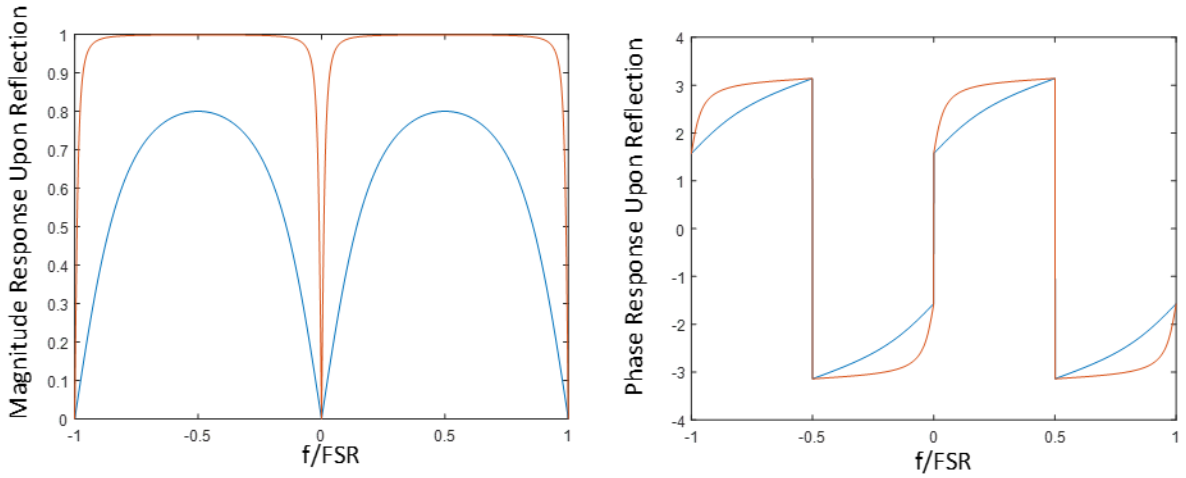

Figure 7 FPE magnitude (left) and phase (right) response upon reflection as a function of detuning of incident laser frequency from the passband for FPEs of finesse 2 (blue) and 30 (red)

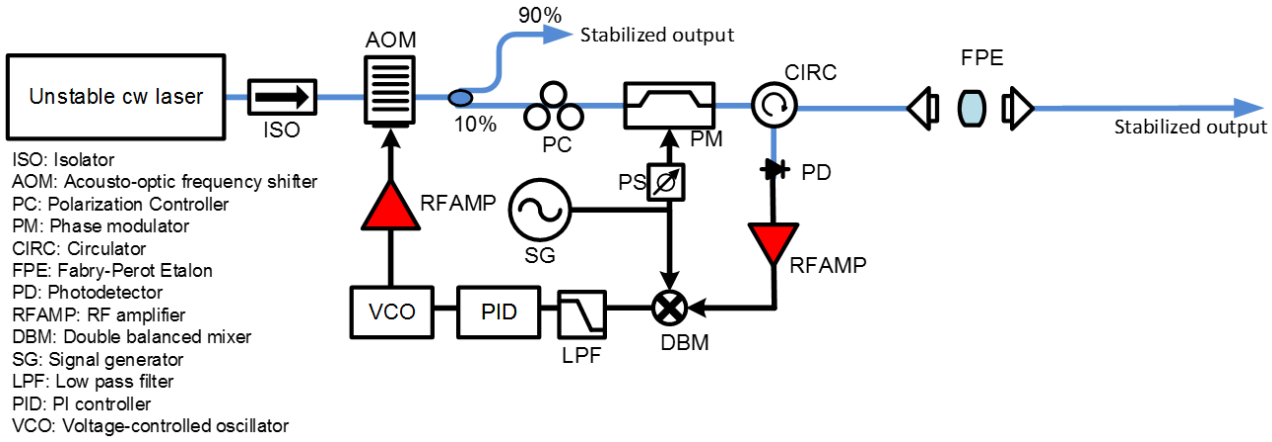

Figure 8 Conventional PDH CW laser frequency stabilization setup

To use the PDH technique in the nested cavity laser architecture, some laser output light is tapped off to be used for stabilization (Figure 9). This portion of light is phase modulated and injected back into the laser cavity orthogonally polarized to the laser polarization state using a polarization beam splitter. The reflected PDH light is coupled out of the cavity using the same polarization beam splitter. Because PDH is being performed on several frequency components at

once, the laser error signal does not take the form of the classic PDH error signal, but the multi-combline PDH error signal does have a linear region where locking is performed. Whereas conventional PDH feeds back to an AOM to shift the CW laser frequency, in this case, the feedback point is to a piezoelectric fiber stretcher to compensate for changes to the optical length of the cavity which result from environmental disturbances.

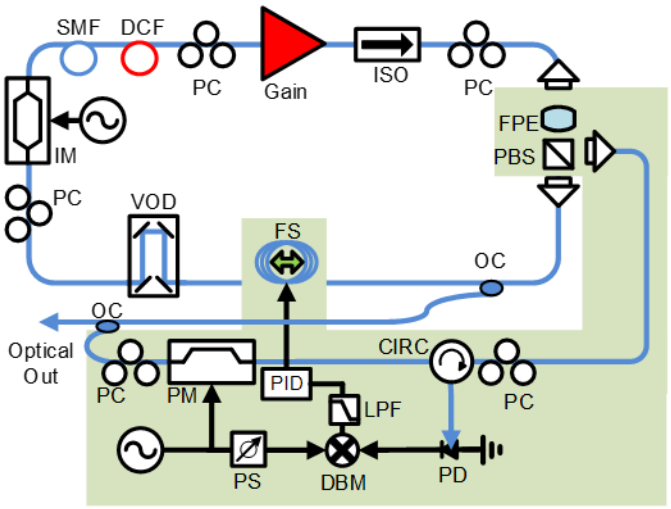

Figure 9 Multi-combline PDH setup implementation in a ring laser cavity (in green shading).

2.4 Dispersion compensation

Finally, the standard single mode fiber (SMF-28) which makes up most of the laser cavity has anomalous dispersion, which results in passive cavity modes walking off from the fixed spacing defined by the signal which drives active mode-locking operation. As such, it may be necessary to incorporate some form of dispersion compensation into the laser setup, whether that is in the form of an advantageous ratio of SMF and dispersion compensating fiber (DCF) [14] or a pulse-shaper [30], which can provide line-by-line amplitude and phase control for combline spacing greater than a few gigahertz. Both of these approaches adds cavity loss (0.5 dB per fusion

splice in addition to propagation losses for DCF, ~6dB for the line-by-line pulse shaper), so this may not be feasible for all systems.

2.5 Summary of the Nested Cavity Architecture

All building blocks for the nested cavity architecture have been introduced, and the full setup is shown in Figure 10 and described as follows.

An SOA is used for cavity gain. Because an SOA chip has low cavity Q, a long external fiber cavity is used to obtain narrow axial mode linewidth, and cavity loss is actively modulated at a harmonic of the fundamental cavity frequency, thereby achieving the high repetition rate of a short cavity and the narrow mode linewidth of a long one. To mitigate the supermode noise associated with harmonic mode-locking, an FPE is nested within the long cavity and provides optical filtering. The harmonic mode-locking rate is chosen to match the FSR of the FPE, and a VOD is used to coarsely match the length of the fiber cavity to a harmonic of that of the FPE.

The long fiber cavity is susceptible to environmental disturbances, so a PDH loop using the intracavity FPE as a length reference is used to provide feedback to a piezoelectric fiber stretcher (FS) to stabilize the cavity length for long term operation. A free-space PBS aids in launching PDH light orthogonally polarized to the laser state of polarization to the FPE and redirecting it out of the laser cavity for PDH stabilization. The phase modulation rate for the PDH loop is chosen so that sidebands lie well within the reflection band of the FPE and are far from resonant with the rest of the laser cavity.

Because standard single mode fiber (SMF-28) fiber has anomalous dispersion, some added normal dispersion in the form of dispersion compensating fiber (DCF) or a line-by-line dispersion control element such as a Finisar Waveshaper may be desired to flatten the dispersion in the

wavelength region of interest in order to increase the optical region where fiber cavity modes are equally spaced for broad bandwidth operation. Polarization controllers (PCs) are placed around the laser cavity to control the state of polarization before polarization-sensitive elements.

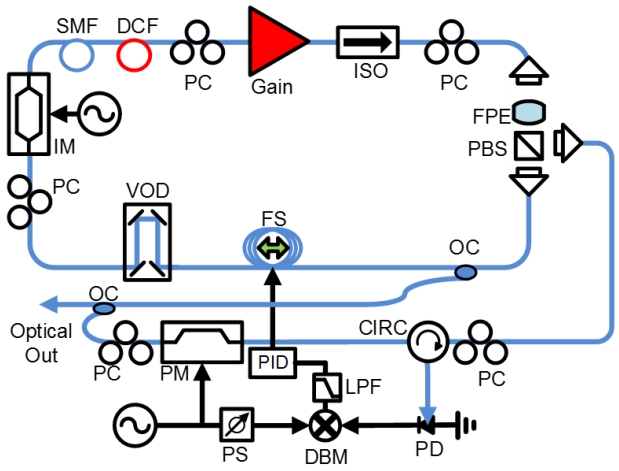

Figure 10 Full nested cavity architecture: ISO (Isolator), PC (polarization controller), FPE (Fabry–Pérot Etalon), PBS (polarization beam splitter), OC (optical coupler), FS (piezoelectric fiber phase shifter), VOD (free-space variable optical delay), IM (Mach-Zehnder intensity modulator), SMF (standard single mode fiber), DCF (normal dispersion fiber), PM (phase modulator), CIRC (circulator), PD (photodetector), DBM (double balanced mixer), PS (RF phase shifter), LPF (low pass filter)

2.6 Previous Work

The first demonstration of using an FPE as both an intracavity optical filter for supermode suppression and for cavity length stabilization was done by Gee et al. in 2005 [12] with an FPE of finesse 150 and FSR of 10 GHz. Since then, improvements in finesse by two orders of magnitude have been demonstrated (Finesse ~ 10^3: [28, 41] and Finesse ~ 10^4: [29, 33, 42]). Increasing gain saturation power has also been explored [14, 37, 42].

CHAPTER 3: OPTICAL AND RF PERFORMANCE ASSOCIATED WITH CAVITY LENGTH AND INTRACAVITY POWER

This source architecture has been motivated by applications which benefit from linewidth, stability and phase noise performance. In the following sections, the measurement techniques for these metrics are introduced. From theory, the two cavity parameters of intracavity power and passive resonance width are identified as variables which influence the three metrics. Those two cavity parameters can be controlled through gain saturation power and cavity length. FPE finesse is also found to be necessary to change alongside cavity length to maintain effective supermode suppression, bringing the number of varying cavity elements to three. From this analysis, several system configurations were determined in order to study the interplay of these elements.

3.1 Optical performance

3.1.1 Linewidth

The lower limit for the linewidth of a CW laser is given by the modified Schawlow-Townes linewidth equation [43, 44]:

$$\Delta\nu_{laser} = \frac{h\nu\ \theta\ l_{tot}^2}{4\pi\ T_{rt}^2\ P_{out}}$$

where ν is the laser frequency, θ is the spontaneous emission factor, l_{tot} is the total parasitic loss in the cavity including the output coupler, T_{rt} is the round-trip time of the cavity, and P_{out} is the output power. This relationship can be simplified using the following expression for passive cavity resonance width:

$$\Delta\nu_{passive} = \frac{l_{tot}}{2\pi\ T_{rt}}$$

Relating the laser linewidth to the passive resonance width:

$$\Delta\nu_{laser} = \frac{\pi\, h\nu\, \theta \left(\Delta\nu_{passive}\right)^2}{P_{out}}$$

Note that passive cavity resonance width varies as the inverse of cavity length, while laser linewidth varies as the inverse of the square of cavity length.

In 1985-86, P. T. Ho et al. demonstrated that, perhaps counterintuitively, the optical linewidth for an extended cavity semiconductor laser is the same for CW and for mode-locked operation. Despite the average power per combline being lowered by the number of comblines, the fixed phase relationship across the frequency comb grants the certainty that the phase of a single combline does not vary independently [45, 46], so the Schawlow-Townes limit does hold for a mode-locked laser. However, the minimum achievable linewidth of a semiconductor gain-based laser is increased from the Schawlow-Townes limit due to coupling between intensity and phase noise as the refractive index in the gain medium varies with carrier density. This is accounted for by the addition of a term including a linewidth enhancement factor α in the equation above [47-49]. Typical values for α in semiconductor quantum well devices are 2-6 [49]. The modified equation linewidth limit in a semiconductor laser becomes:

$$\Delta\nu_{SC\ laser} = \frac{h\nu\, \theta\, (1+\alpha^2) l_{tot}^2}{4\pi\, T_{rt}^2\, P_{out}} = \frac{\pi\, h\nu\, \theta\, (1+\alpha^2) \left(\Delta\nu_{passive}\right)^2}{P_{out}}$$

Reviewing this final expression, the factors which can be easily controlled in the system under study are power and passive cavity resonance width.

Linewidth can be measured using a delayed self-heterodyne measurement, however this typically requires a path length delay of longer than the coherence length. For sub-kHz linewidths, this would require a delay of several hundred kilometers of fiber. Instead, in this work, the laser is

beat with a reference laser which is known to be narrower in linewidth and is close enough in optical frequency to produce a beat note within the bandwidth of the measurement electronics. For these measurements, a commercially available narrow linewidth laser at center wavelength 1551 nm is used and sets the desired operating wavelength of the mode-locked laser to achieve spectral overlap. The heterodyne beat note is Lorentzian in lineshape, the result of the convolution of two Lorentzian laser tones. As such, its width is the sum of the widths of the two laser tones which produced it, so the width of the laser being tested can be assumed to be less than the heterodyne beat note width by the width of the reference CW laser.

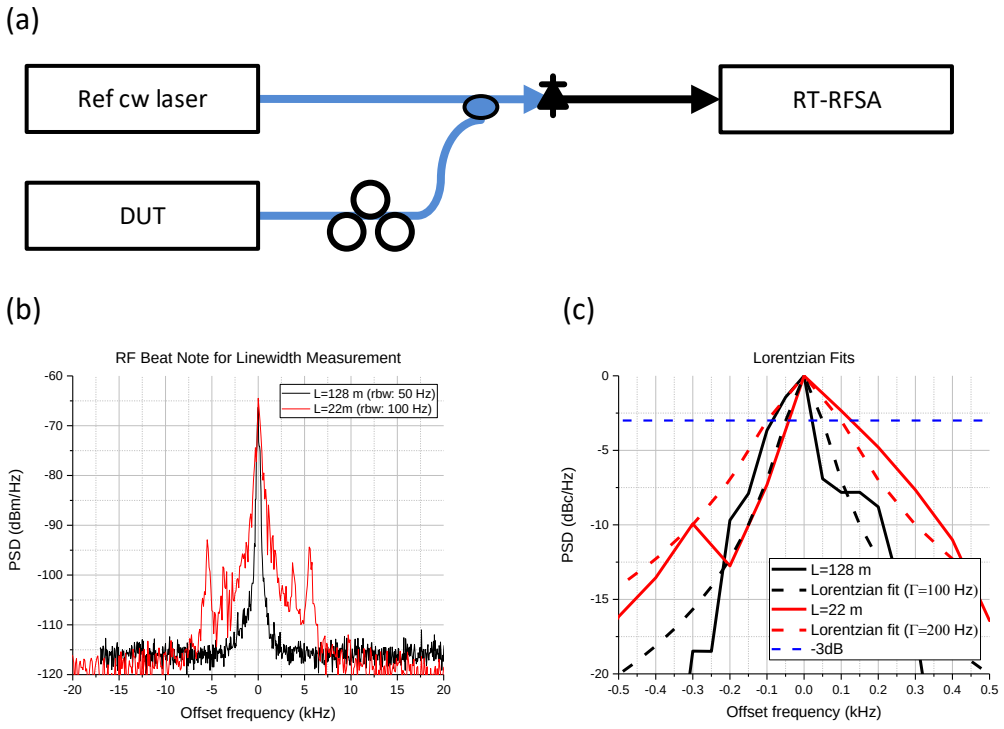

Figure 11 (a) heterodyne beat measurement setup for linewidth measurement. RT-RFSA: Real-Time RF Spectrum Analyzer; (b) linewidth measurement data for a short cavity (red) and a long cavity (black); (c) close-in view of the same data as (b) with Lorentzian fits in dashed lines. Asymmetry in data traces is thought to be a result of beatnote movement during data capture and the operation near the resolution limit of the reference source used in this measurement (30 Hz).

This measurement has been performed to characterize the linewidth of two nested cavity lasers with different cavity lengths. Both systems used an SOA as the gain medium. The results are shown in Figure 11. The heterodyne beatnote linewidth of the 22 m and 128 m systems was measured at 200 Hz and 100 Hz, respectively, using Lorentzian fits to the heterodyne beatnote data. With the reference CW laser being 30 Hz in width, the laser under test linewidths can be calculated at 170 Hz and 70 Hz. This is a 3.8 dB decrease in linewidth for a 7 dB increase in length. This is close to the expected inverse quadratic relationship between laser linewidth and cavity length discussed above.

3.1.2 Optical combline stability

A single combline's long-term frequency stability can be measured with the Allan deviation measurement technique. The Allan deviation gives a distribution of fractional frequency deviation for a specified range of timescales [50, 51]. Unlike standard deviation, it is suitable for datasets in which consecutive data points are related to each other, where the value of one data point depends on the value which comes before it. For this reason, an Allan deviation requires a zero-deadtime frequency counter. The frequency counter receives the RF tone to be measured and counts the number of zero crossing events during a given block of time τ. The average frequency for that time bin is computed, and this action is repeated for N blocks. Subsequent time blocks must have no deadtime between each other or the measured deviation will be artificially increased. The Allan deviation for a given timescale τ is computed as follows:

$$\sigma_y(\tau) = \sqrt{\sum_{k=1}^{N} \frac{1}{2}\left(\bar{f}_{k+1} - \bar{f}_k\right)^2}$$

Like the linewidth measurement, the measurement setup for Allan deviation is a heterodyne beat scheme. In this case, the reference needs to have long-term stability surpassing that of the mode-locked laser. A CW laser PDH-locked to an FPE which has superior length stability over the device under test or a frequency comb with locked repetition rate and carrier envelope offset frequency would be appropriate.

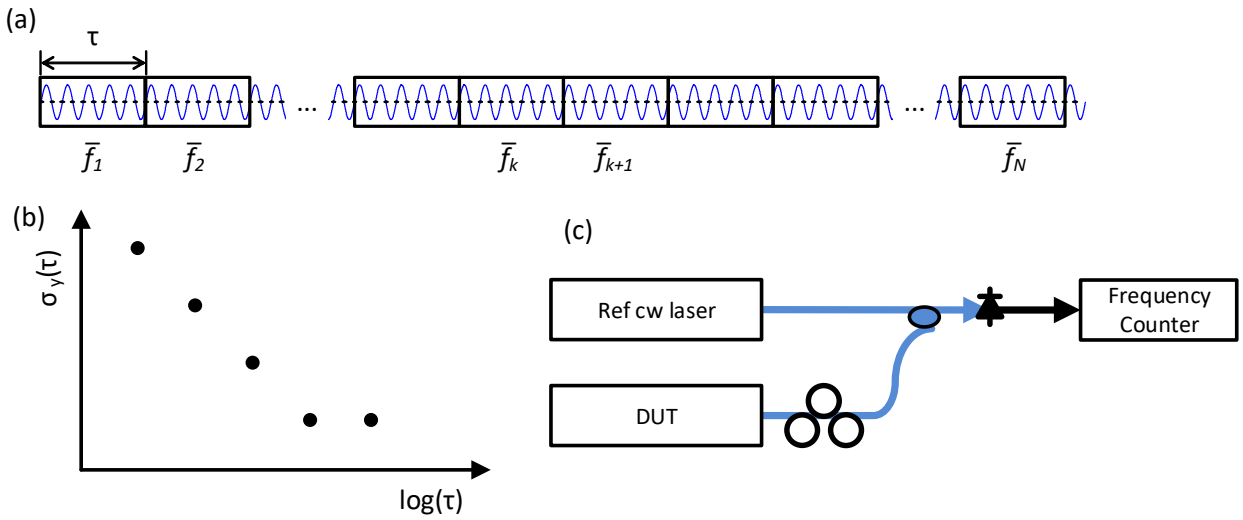

Figure 12 (a) Allan deviation: a frequency counter counts the number of zero crossing events during consecutive time windows of length τ and computes the average frequency during each bin; (b) Computation of the Allan deviation gives deviation characteristics at different timescales; (c) measurement setup

The heterodyne setup in Figure 12(c) will measure the deviation of the RF tone at the frequency difference between the CW laser and the 10 GHz frequency comb under test, which is less than Nyquist frequency (5 GHz). However, the RF frequency deviation measured represents deviation of the optical mode at ~193 THz, so while the fractional stability of the RF tone may not be of impressive performance, it represents the relative stability of an optical tone that is better by

the ratio between the optical frequency of the laser mode and the RF beat note, which is at least 5 orders of magnitude.

$$\sigma_y(\tau)\big|_{meas.} = \frac{(\Delta f)_{beat}}{f_{beat}} \; ; \qquad \sigma_y(\tau)\big|_{opt} = \frac{(\Delta f)_{beat}}{f_{opt}} = \frac{f_{beat}}{f_{opt}}\sigma_y(\tau)\Big|_{meas.}$$

At short timescales, the frequency stability is related to linewidth. Theoretically, at long time scales the frequency stability should be influenced by FPE finesse; a high finesse indicates greater frequency selectivity, which should allow a tighter PDH lock and cause a lower fractional frequency deviation.

As yet, long term stability has not been successfully measured for the nested cavity architecture presented here. The long term stability performance at long timescales (τ>100 s) of the nested cavity architecture likely depends on how well the PDH electronics can keep the comb locked to the FPE, and on the aging rate of the ultra-low expansion quartz spacer in the FPE assembly.

3.2 RF performance: residual phase noise

Phase noise can be difficult to measure for high repetition rate pulse trains. With enough measurement bandwidth, one can look at the noise skirt on a high harmonic of the photodetected pulse train and easily see the demarcation between amplitude noise, which is constant with harmonic number, and phase noise, which grows quadratically with harmonic number. For pulse repetition rates of 10s of gigahertz, the relative phase noise measurement is a solution for the bandwidth limitations of the direct photodetection measurement. An oscillator signal can be written as a sinusoid with amplitude V_0, frequency ω, and time-varying amplitude and phase fluctuations.

$$V(t) = V_0(1 + \alpha(t))\cos[\omega t + \varphi(t)]$$

Given two signals of equal frequency, to measure their relative phase noise independent of amplitude noise of the second signal, the two signals can be mixed at quadrature, resulting in two sinusoids at DC and doubled frequency. Here, the amplitude and phase noise terms represent the relative amplitude and phase noise between the two signals.

$$V_{mixed} = V_0^2[1+\alpha(t)]\cos(\omega t)\cos\left[\omega t+\varphi(t)+\frac{\pi}{2}\right]$$

$$V_{mixed} = V_0^2[1+\alpha(t)]\left[\cos\left(2\omega t+\varphi(t)+\frac{\pi}{2}\right)+\cos\left(-\varphi(t)-\frac{\pi}{2}\right)\right]$$

$$V_{mixed} = -V_0^2[1+\alpha(t)]\{\sin[2\omega t+\varphi(t)]+\sin[\varphi(t)]\}$$

Filtering out the doubled frequency term with a low pass filter, and assuming that for a good oscillator, $\alpha(t) << 1$ and $\phi(t) << 1$, the resulting voltage signal is close to a zero-offset DC value with frequency content that is linearly related to the relative uncorrelated phase noise $\varphi(t)$. Measuring the frequency content of $\varphi(t)$ gives the single-sideband phase noise, and integration from a low offset frequency out to Nyquist frequency gives the statistical rms value of timing jitter between consecutive pulses.

$$T_j = \frac{1}{2\pi f_{rep}}\sqrt{2\int_{f_0}^{f_1} S_\varphi(f)df}$$

The factor of two inside the square root accounts for both upper and lower sidebands of the carrier frequency.

A relative noise measurement is suitable when there are two identical but uncorrelated systems to measure against each other so that it can be reasonably assumed that half of the noise comes from each source. Absent in the equations above is the correlated phase noise, which would not cancel out in the 2ω term, but is not present after low pass filtering. In this case, obtaining two identical FPEs to build two nested cavity sources would be unfeasible. However, one can

easily perform a residual phase noise measurement (setup shown in Figure 13(a)) where the laser output is measured against the signal driving the active mode-locking process.

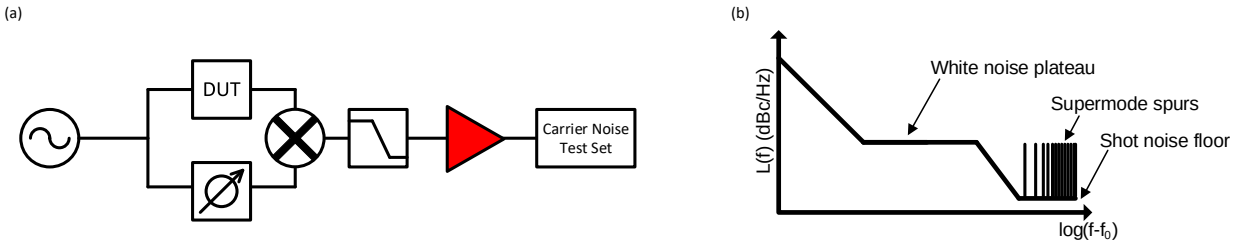

Figure 13 (a) Residual phase noise setup (b) illustrated example of a typical single-sideband phase noise measurement from a harmonically mode-locked laser.

A residual phase noise measurement by definition measures uncorrelated noise between the two paths. In the case where the DUT is noisier than the RF source, the residual phase noise measurement is completely dominated by the DUT noise. However, when measuring a high quality factor laser, there can be a filtering effect, where there are portions of the single-sideband phase noise spectrum which are dominated by the noise in the RF source which have been filtered out of the DUT arm and are thus uncorrelated upon mixing [52]. If relying on a residual phase noise measurement to characterize timing performance, it is therefore important to choose an RF source with better phase noise performance than the device under test.

Shown in Figure 13(b) above is a cartoon phase noise plot of a mode locked laser with some salient features pointed out. First, the shot noise floor at higher offset frequencies can be decreased by having more power incident on the photodetector to generate more photocurrent. Supermode noise spurs, a side effect of harmonic mode-locking, can be suppressed with an appropriately high-finesse etalon. If additional length is added to the cavity, a higher finesse FPE will be required to achieve the same amount of suppression. Finally, the white noise plateau has a corner or "knee" frequency which is related to spontaneous emission (and thus the passive cavity resonance width),

and decreasing the width of the passive cavity resonance by increasing cavity length or decreasing the output coupling ratio can push the corner frequency to lower offset frequencies. This effect is visible in the residual phase noise measurements shown in Figure 14. When cavity length was increased from 22 m to 351 m, the supermode offset frequency spacing decreased from 9 MHz to 570 kHz, and the white noise plateau corner frequency was pushed in from 100 kHz to 10 kHz.

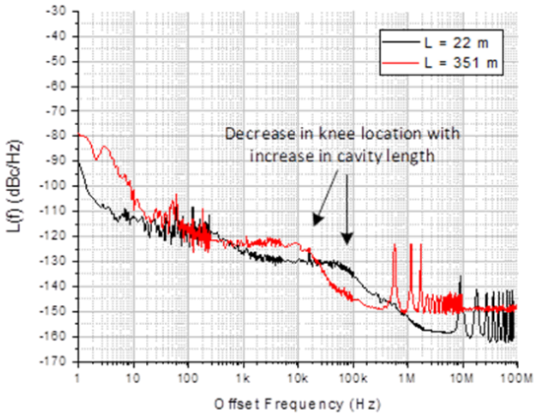

Figure 14 Residual phase noise measurements for two systems of different length, showing the decrease in white noise corner frequency and in supermode spur offset frequency. The short cavity's phase noise performance (black) was also shown in Figure 5 to illustrate supermode noise spurs in harmonic mode-locking.

3.3 Proposed systems

In the previous two sections, passive cavity resonance width and intracavity power were identified as two cavity parameters in the nested cavity architecture contributing to the linewidth, stability, and RF phase noise performance. A lower passive cavity resonance width decreases the white noise corner frequency of an RF phase noise measurement and the linewidth of an optical mode. In an effort to have enough output power to drive down the shot noise floor of the phase noise measurement, cavity length is the parameter chosen over cavity Q to vary the passive cavity resonance width. A higher FPE finesse will enable more cavity length to be added without

suffering supermode noise and may also improve Allan deviation. The results from the data shown in Figure 14 Residual phase noise measurements for two systems of different length, showing the decrease in white noise corner frequency and in supermode spur offset frequency. The short cavity's phase noise performance (black) was also shown in Figure 5 to illustrate supermode noise spurs in harmonic mode-locking. and in Figure 11 are gathered in Figure 15 below along with some data from previous work by Yilmaz et al. This decrease in linewidth and white noise corner frequency is extending the work done by Yilmaz et al. who measured the relationship with cavity length for linewidth and knee location in an extended cavity using semiconductor gain media and free-space instead of fiber for the external cavity [15].

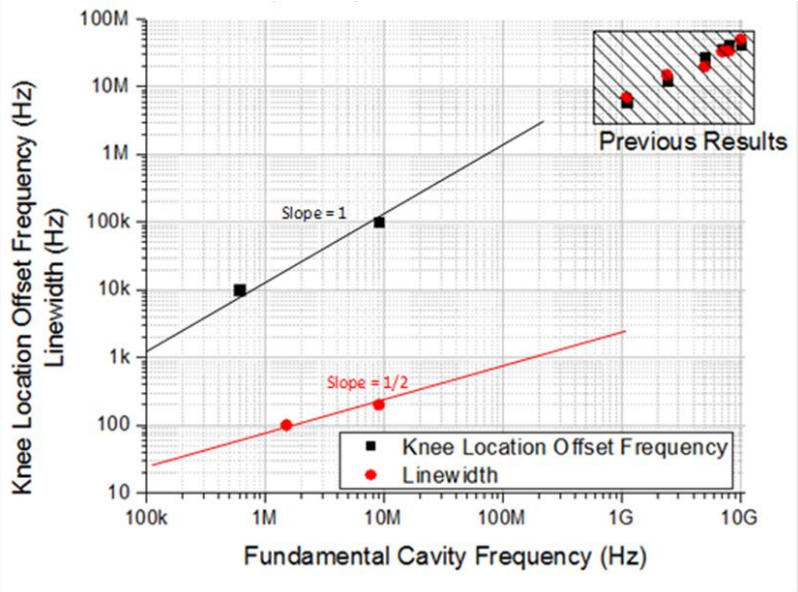

Figure 15 White noise corner frequency (black) and linewidth (red) dependence on cavity length and square of cavity length, respectively. The four new data points agree with the predictions made about the relation of laser linewidth and passive resonance width to cavity length in CHAPTER 2:. Data in "Previous Results" shaded box taken from Yilmaz et al [15]

High intracavity power will result in greater output power to drive down the shot noise floor of the RF phase noise measurement and decrease the laser mode linewidth. Varying

intracavity power could be done by increasing gain saturation power or by decreasing the output coupling ratio. Because decreasing the output coupling ratio would result in increased cavity loss (and thus a change to the passive cavity resonance width), gain saturation power was chosen to influence intracavity power in an effort to keep those two parameters as independent as possible. To increase gain saturation power, a novel semiconductor gain medium with high saturation power can replace the SOA as gain medium. Figure 16 shows a comparison of gain saturation for a commercially available SOA and a slab-coupled optical waveguide amplifier (SCOWA), a semiconductor-based amplifier with a unique cross-sectional geometry to guide the optical mode with low waveguide confinement and low overlap with the active quantum well region [53]. This amplifier has low gain, but high saturation power due to the reduction in nonlinear effects allowing a higher maximum pump current. Using this device in a laser means that the laser cavity cannot tolerate as much loss as the conventional SOA-based laser. But if losses are kept low, the SCOWA-based laser has the potential for an increase in intracavity power of ~9 dB, equal to the difference in saturation output powers between the two compared gain media [14].

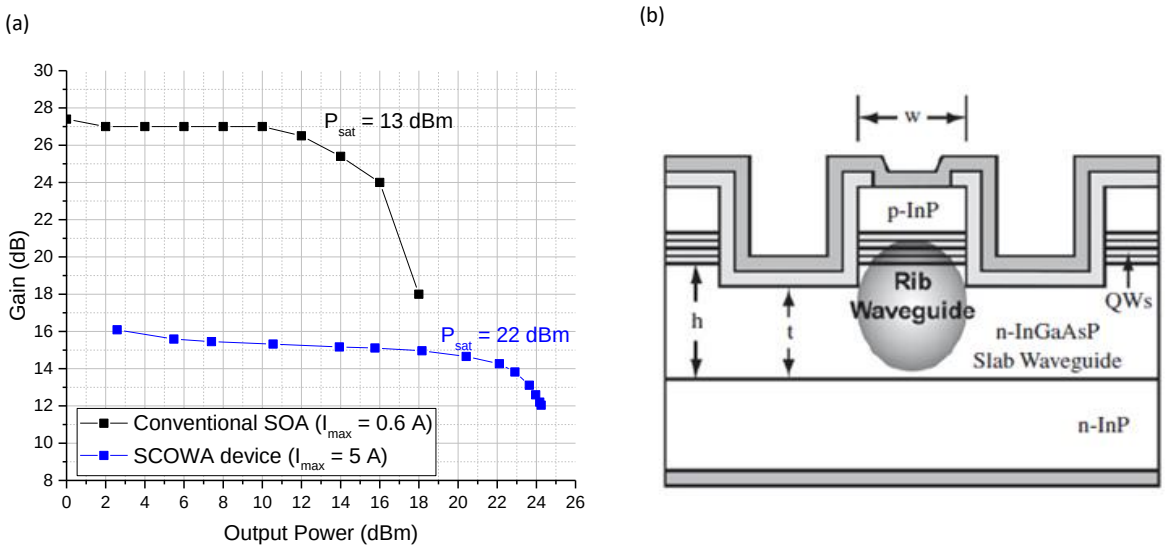

Figure 16 (a) Gain saturation curves for a commercially available SOA device and for the SCOWA device driven at their respective maximum rated currents (b) SCOWA device cross-section showing low optical mode confinement and overlap with the active gain region [53]

Thus far, the three cavity elements of length, gain saturation power, and FPE finesse have been identified for architecture variables which determine phase noise, linewidth, and stability properties. In setting out to realize the system with the most advanced parameter values (long cavity, high gain saturation power, high finesse FPE), some unexpected effects were observed that warranted further study. The main thrust of this research was entering the regime of the high finesse FPE, so four system configurations (short and long cavities, low and high gain saturation powers) were proposed for study. Because it was predicted that finesse may play a role in long timescale Allan deviation due to its higher frequency selectivity, one system of low finesse FPE was also studied.

Table 1 Enumeration of the proposed systems to measure

ID	Gain element	Cavity length	Etalon finesse
1	SOA	Short	10k
2	SOA	Long	10k
3	SCOWA	Short	10k
4	SCOWA	Long	10k
5	SCOWA	Short	1k

System 4 (SCOWA, long cavity, 10k finesse FPE) in particular, where both gain saturation power and cavity length/finesse have been pushed forward by an order of magnitude, is the configuration which instigated some of the study of trade-offs contained in this document. The full characterization of all of these systems details the trade-offs associated with these cavity parameters experimentally.

Although this architecture, and even some of these configurations, have been studied previously, no one system configuration has had the full set of diagnostics performed. In order to understand the interplay between the three cavity elements of gain saturation power, length, and FPE finesse, we have fully characterized each of these configurations to shed light on this interplay.

CHAPTER 4: TRADE-OFFS ASSOCIATED WITH LENGTH, GAIN SATURATION, AND FPE FINESSE

In the previous chapter, the plan of study of five cavity configurations varying saturation power, length, and FPE finesse was laid out in order to fully understand the interplay between them. There are some trade-offs between these elements which may not be immediately obvious which are explored in the following sections.

4.1 Cavity length and operating bandwidth

The anomalous dispersion of the fiber cavity causes cavity mode spacing to vary across the spectrum. However, the ideal spacing is fixed by the signal driving mode-locking operation, so the range over which these two grids match up may be limited, resulting in an upper limit to operation bandwidth. Adding cavity length with standard SMF fiber shortens this achievable bandwidth significantly. In previous systems, some of this dispersion has been counteracted by also adding an appropriate length of DCF or by inserting a line-by-line pulse shaper to flatten the dispersion of the cavity [14, 30].

In the systems with SOA gain, the cavity can tolerate the additional loss of the added DCF (propagation loss of 0.3 dB/m along with connector losses of 0.8-1.4 dB per connection due to mode field diameter mismatch; core sizes of SMF and DCF are 9 μm and 5-6μm, respectively) or of the pulse shaper (6 dB). However, adding dispersion compensation in the SCOWA-based systems can prove to be challenging, especially in the longer cavity configurations, if high intracavity power is the goal. In the work done by Davila-Rodriguez et al. with dispersion compensation of a short SCOWA-based laser, the bandwidth was successfully broadened from 2 nm to 10 nm with the addition of DCF [14]. However, the phase noise measurement showed an

increase in phase noise of >5 dBc/Hz at offset frequencies up through the white noise plateau. Timing jitter integrated through Nyquist was increased from 10 fs to 14 fs. The linewidth of the all-anomalous cavity and the dispersion compensated cavity was not directly compared because there was no suitable reference at the time, but given the increase in white noise in the phase noise measurement resulting presumably from an increase in cavity loss, it's reasonable to predict that the linewidth also suffered.

4.2 Gain and saturation power

The high saturation gain medium of the SCOWA is promising for significantly increasing intracavity power (Figure 16). The gain of the SCOWA is much lower than that of the SOA, so using the SCOWA puts a constraint on the loss of other cavity elements in order for laser operation to be possible.

Table 2 contains a summary of the loss budget of the system. For the shorter cavity case, a small length of DCF with SMF patch cords was selected to provide some dispersion compensation to broaden the operating bandwidth. For the longer cavity cases, a spool of fiber of total length 81 m conprising an appropriate ratio of SMF and DCF was selected for use both for dispersion compensation and for adding length to the cavity. The loss in both cases is due mainly to the mismatch between mode field diameters at the fusion splice points between SMF and DCF.

Table 2 Loss budget of cavity elements (excluding gain medium)

Component	**Measured insertion loss (dB)**	**Rated insertion loss (dB)**
ISO1	-0.8	-0.8*
PBS	-0.6	-0.6*
OC	-0.5	-0.5*
VOD	-1.3	-1*
FS	-0.5	0*
IM	-3	-2.9*
ISO2	-0.8	-0.8*
Etalon	-0.9	-1.1
Added fiber spool (longer cavity case)	-2.1	-1.6*
Short DCF length (shorter cavity case)	-1.1	-1.0 *
Total cavity loss	-10.5 (Long cavity case: -11.5)	-8.7 (Long cavity case: -9.3)*

*plus additional connector losses via mating sleeves

4.3 Length and free-running stability

Discussed in Section 3.2, supermode noise spurs can contribute significantly to timing jitter. Using a FPE can suppress the supermode noise spurs to below the noise floor of a phase noise measurement. However, cavity length can only be increased so much before the nearest supermode neighbors start to creep into the etalon passbands and show up in a phase noise measurement. If these are to be suppressed, a higher finesse FPE will need to be used. Thus far, the main challenge that comes with increasing FPE finesse is an increased instability in the free-running state. Because the laser cavity with a high finesse FPE is very frequency selective, laser operation is extremely

intermittent if it isn't already locked. Some stability in the free-running state is necessary in order to perform polarization alignment, and to obtain an error signal and subsequently PDH-lock the system.

The trade-offs discussed in this chapter can have cascading effects. In the following chapter, these trade-offs are experimentally demonstrated by studying the interplay of cavity length, gain saturation power, and FPE finesse.

CHAPTER 5: NOTABLE RESULTS

The following subsections contain the performance data for each individual system. The subsequent section will discuss the trends observed across systems due to the changes in cavity elements.

5.1 System Performance

5.1.1 System 1: SOA, short cavity, 10000 finesse FPE

The fundamental cavity frequency for this configuration was ~17 MHz and the average output power was measured to be ~5 mW in the mode-locked state, giving an intracavity power of ~50 mW. Figure 17 shows RF and optical output characterization data. The optical spectrum spans 4.5 nm and the pulses are compressible to autocorrelation width of 2.6 ps, or 1.4 times transform-limited (the transform limited autocorrelation width calculated for the optical spectrum in Figure 17(a) is 1.8 ps). On the photodetected RF spectrum, the nearest supermode noise spur at 17 MHz is suppressed below the noise floor. The sampling scope trace shows a well-behaved 10 GHz pulse train, with measured pulse widths limited by the bandwidth of the photodetector and sampling head.

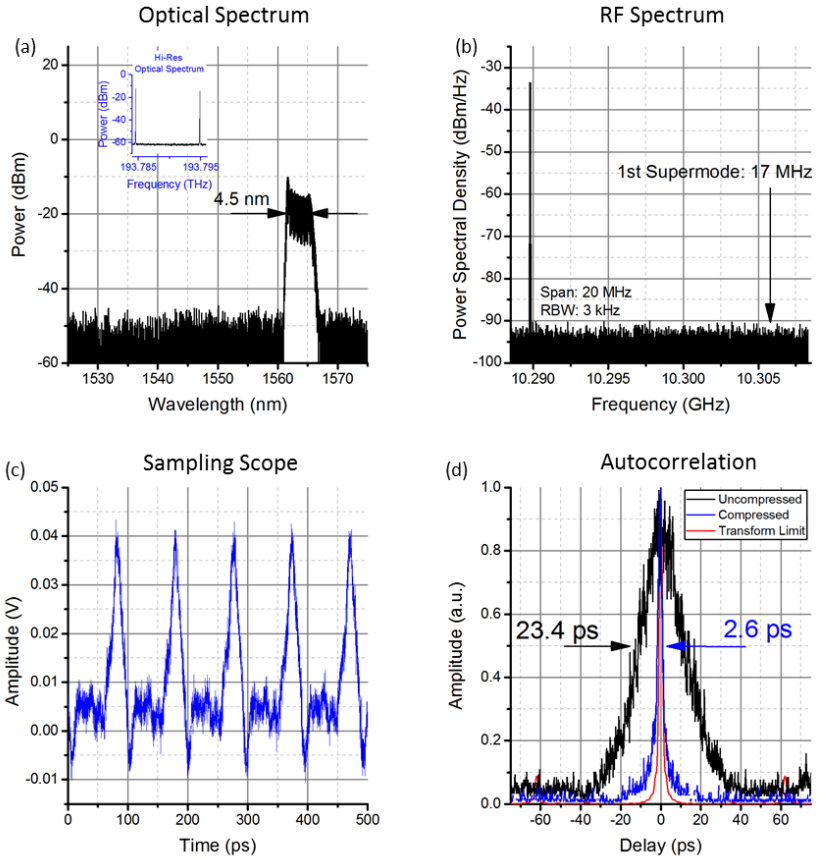

Figure 17 Optical and RF characterization data for System 1 (SOA, short cavity, 10k finesse FPE). (a) Optical spectrum; (a, inset) Hi-res optical spectrum; (b) photodetected RF spectrum; (c) sampling scope trace of photodetected compressed pulses; (d) autocorrelation for uncompressed (black), compressed (blue) and transform-limited (red) pulses

Figure 18(a) shows the linewidth of an optical combline as measured by heterodyne beat experiment as discussed in Section 3.1.1. A Lorentzian fit with FWHM of 1.3 kHz with an added -70 dBc/Hz noise floor is shown for visual aid. The Allan deviation, normalized to the optical frequency of 193.4 THz, reaches a minimum fractional frequency deviation of 5×10^{-13} at an averaging time of $\tau = 30$ ms.

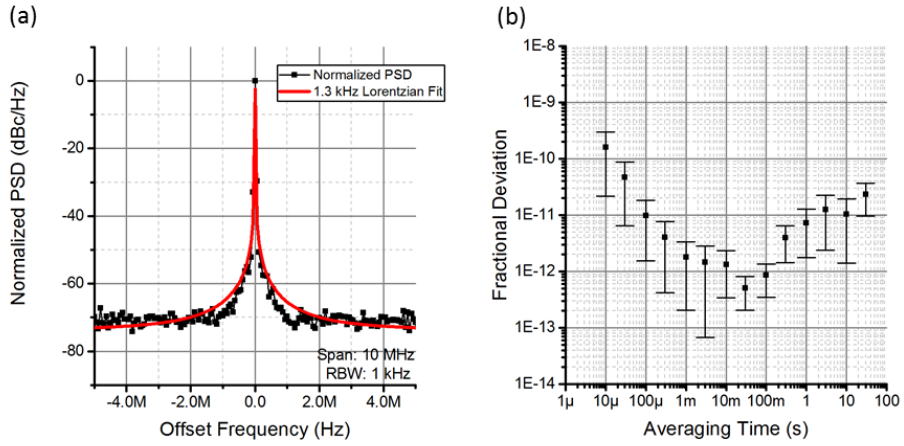

Figure 18 (a) Heterodyne beat with a 100 Hz reference CW laser (black), Lorentzian function with 1.3 kHz FWHM (red). The center frequency of the heterodyne beatnote was 4 GHz (b) Allan deviation data for a heterodyne beat with a cavity-stabilized CW laser, normalized to the optical frequency of 193.4 THz. The center frequency of the heterodyne beatnote was 4.6 GHz.

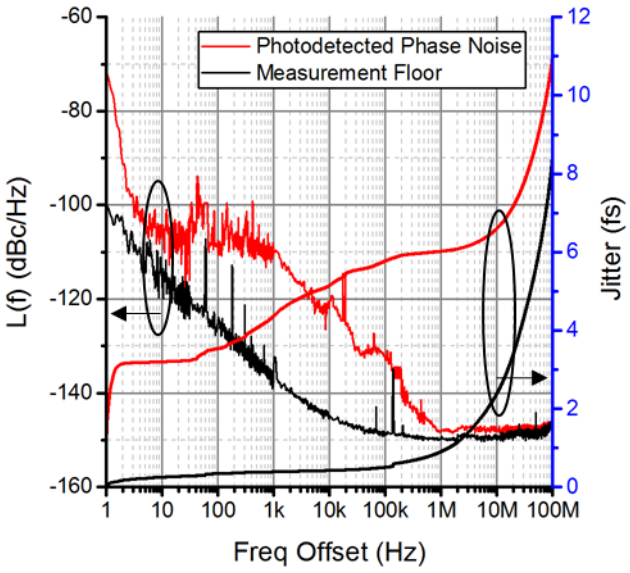

Figure 19 Phase noise data for System 1 (SOA, 10k finesse FPE, short cavity length). Single sideband phase noise (left axis) and integrated timing jitter (right axis) for the photodetected pulse train (red) and for the measurement floor (black).

Figure 19 shows the single sideband phase noise of the photodetected pulse train. The shot noise floor is limited to -148 dBc/Hz by the low power incident on the photodetector, and timing jitter integrated from 1 Hz offset to 100 MHz (Nyquist) is 11 fs (61 fs).

5.1.2 System 2: SOA, long cavity, 10000 finesse FPE

The fundamental cavity frequency for this configuration was 2 MHz, and average optical output power was decreased with the added length of fiber than in System 1 at 2.6 mW (intracavity power approximately 26 mW). Optical bandwidth was measured at 3.5 nm, and pulses were compressible to 1.1 times transform limited autocorrelation width. The first supermode noise spur at 2 MHz was suppressed below the noise floor of the RF spectrum analyzer, and the sampling scope trace shows a well-behaved 10 GHz pulse train.

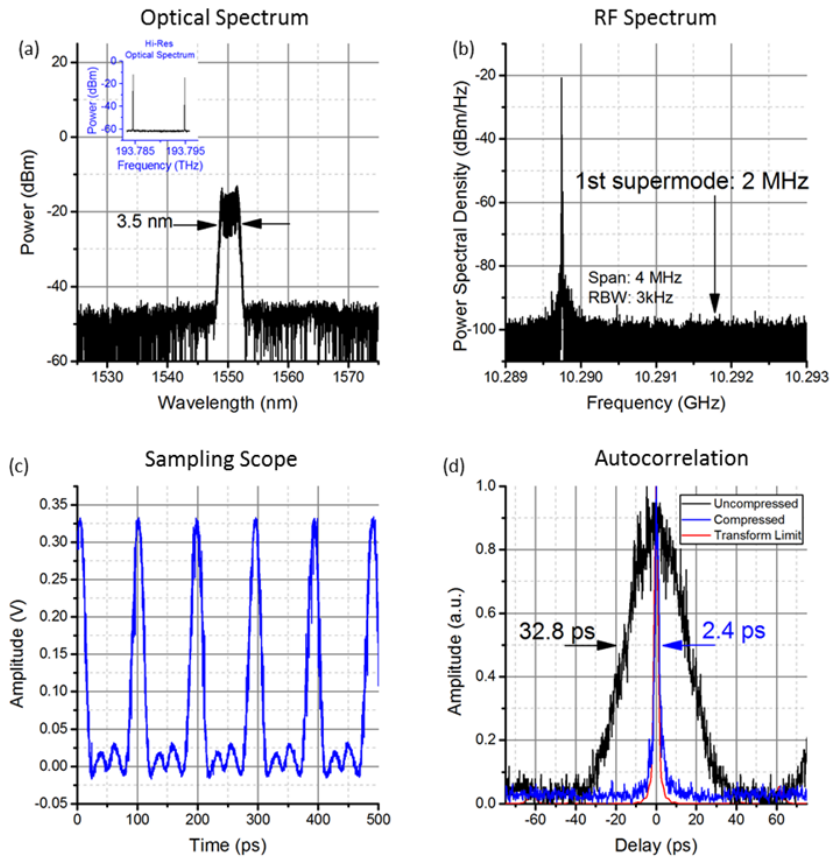

Figure 20 Optical and RF characterization data for System 2 (SOA, Long cavity, 10k finesse FPE). (a) Optical spectrum; (a, inset) Hi-res optical spectrum; (b) photodetected RF spectrum; (c) sampling scope trace of photodetected compressed pulses; (d) autocorrelation for uncompressed (black), compressed (blue) and transform-limited (red) pulses

Linewidth and Allan deviation data are shown in Figure 21. The heterodyne beatnote shows good agreement with a Lorentzian function of 150 Hz FWHM with an added measurement floor of -58 dBc/Hz. The Allan deviation reaches a minimum of 3 x 10^{-12} at τ = 100 ms.

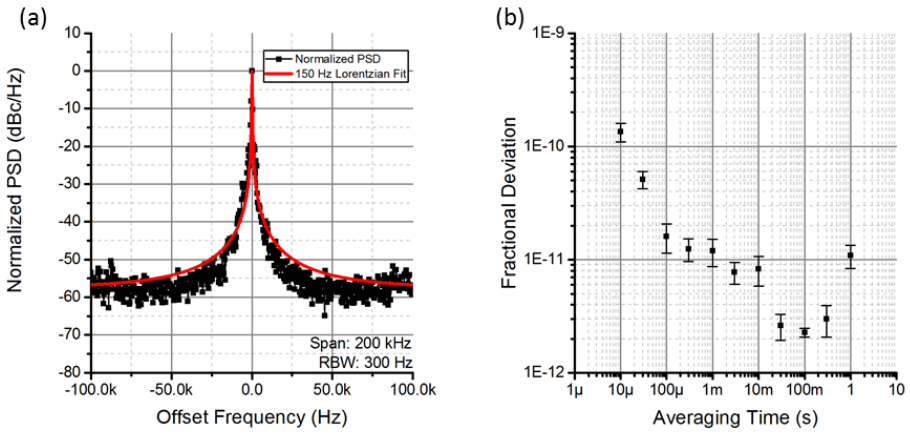

Figure 21 (a) heterodyne beat between a combline from System 2 and a 100-Hz CW reference laser. A 150 Hz Lorentzian function is shown in red for visual aid; (b) Allan deviation measurement of a heterodyne beat with a cavity-stabilized CW laser, normalized to the optical frequency of 193.4 THz

5.1.3 System 3: SCOWA, short cavity, 10000 finesse FPE

Chronologically this was the first short-cavity system to be realized for this work. As a result, the cavity length and SMF/DCF ratio all short cavities was set by optimizing the performance of this system. The cavity length comprised 0.5 m DCF and approximately 12 m SMF, resulting in a fundamental frequency of 16.7 MHz. This frequency lies well into the stopband of the 10k finesse FPE and supermodes were thoroughly suppressed as is evident in the single sideband phase noise spectrum. Average optical output power for this configuration operating in the mode-locked state was 10-12 mW, giving an intracavity power as high as ~120 mW. Figure 22 shows optical and RF characterization of the mode-locked laser output. The optical spectrum spans 4.5 nm in bandwidth, and optical modes have >40 dB OSNR. The RF spectrum of the photodetected output shows a

clean 10.29 GHz tone and suppression of the nearest supermode spur to below the noise floor. The photodetector used for the sampling scope measurement had a bandwidth of 50 GHz, and the measurement of the compressed pulses show a well-behaved 10 GHz pulse train, with pulse widths limited by the photodetector. Autocorrelation measurement shows that the pulses are compressible to near the transform limit (as calculated using the optical spectrum data) of autocorrelation widths of 1.5 ps.

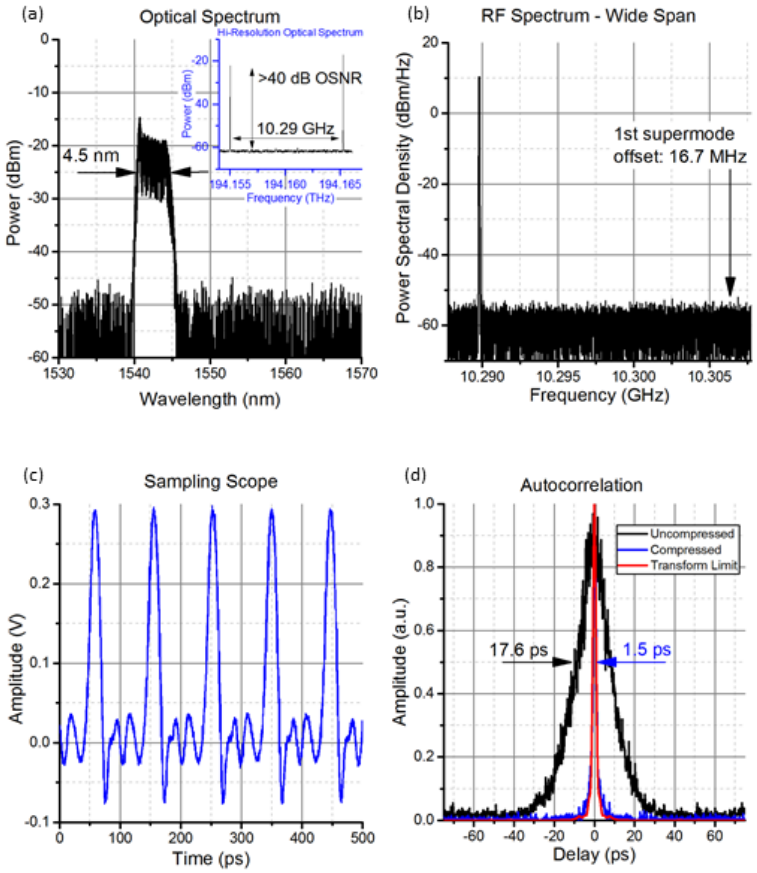

Figure 22 Optical and RF characterization data for System 3 (SCOWA, Short cavity, 10k finesse FPE). (a) Optical spectrum; (a, inset) Hi-res optical spectrum; (b) photodetected RF spectrum; (c) sampling scope trace of photodetected compressed pulses; (d) autocorrelation for uncompressed (black), compressed (blue) and transform-limited (red) pulses

Phase noise and integrated timing jitter are shown in Figure 23. The shot noise limit of this measurement was limited by the average power incident on the photodetector (9 mW) and the fact that pulses were not sent to the photodetector in a compressed state in the interest of preserving power. The shot noise floor is however, decreased from that of the system in Section 5.1.1 due to the increase in average power. The phase noise reaches the shot noise limit before an offset frequency of 5 MHz, and the white noise knee frequency is near 100 kHz. Integrated out to Nyquist frequency, timing jitter is less than 25 fs.

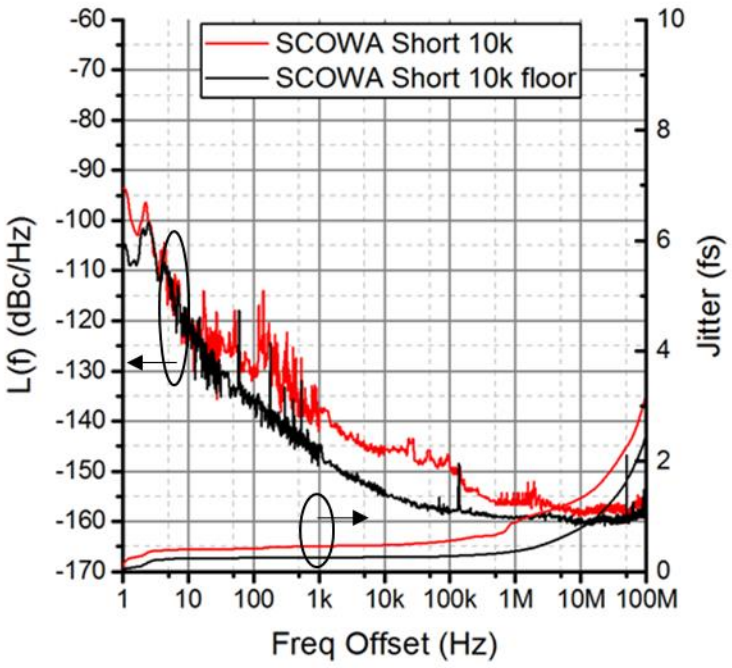

Figure 23 Phase noise data for System 3 (SCOWA, short cavity, 10k finesse): Single sideband residual phase noise (left axis) and integrated timing jitter (right axis) for the photodetected pulse train (red) and the measurement setup noise floor (black)

Linewidth and long term stability are shown in Figure 24 and were measured as discussed in sections 3.1.1 and 3.1.2. The linewidth of the heterodyne beat is nearly limited by the reference 100 Hz CW laser used for the measurement and measures at <150 Hz (A 125 Hz Lorentzian fit with an added noise floor of -55 dBc/Hz is shown for visual aid). The Allan deviation reaches a minimum fractional frequency deviation of 3×10^{-13} at an averaging time $\tau = 30$ ms (corresponding to an absolute deviation of the optical tone of ~70 Hz).

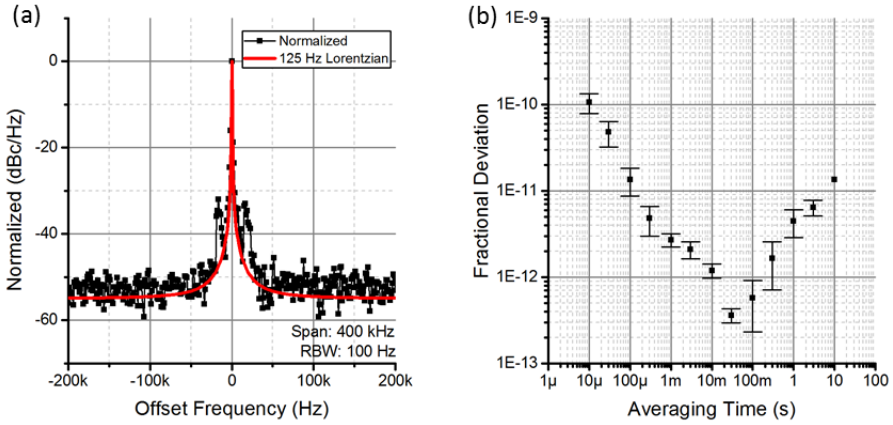

Figure 24 (a) Heterodyne beat between a combline from System 3 and a 100-Hz CW reference laser. A 125 Hz Lorentzian function with an added noise floor is shown in red for visual aid; (b) Allan deviation measurement of a heterodyne beat with a cavity-stabilized CW laser, normalized to the optical frequency of 193.4 THz

5.1.4 System 4: SCOWA, long cavity, 10000 finesse FPE

This configuration was the first attempted, and its initial performance did not show the expected low noise, highly stable characteristics that were expected. It is what drove the direction of the analysis in this dissertation. The fundamental cavity frequency for this configuration is ~2 MHz, and the average optical output power is ~8 mW, giving an intracavity power of ~80 mW. Although the insertion loss of the fiber length was kept low at -1.1 dB, the addition clearly stretched the loss budget of the system. While threshold current for System 3 (SCOWA, short cavity, 10^4 finesse FPE) was near 2 A, the threshold current for this system was nearly 3 A. The system was much more sensitive to polarization drift as well. With the added fiber spool placed directly before the SCOWA, stable PDH-locked operation was not achieved for longer than 60 seconds. This degraded PDH performance resulted both from increased sensitivity to environmental perturbations and from a smaller effective ability to compensate for those environmental disturbances (see section 4.3)

Figure 25 shows the optical and RF characterization data for System 4. The optical bandwidth was 1.1 nm and pulses were compressible to 1.1 times transform limited. The nearest supermode noise spur at 2 MHz offset from the carrier was suppressed to below the noise floor on the RF spectrum of the photodetected pulse train. The sampling scope trace of the photodetected compressed pulses show a well-behaved 10 GHz pulse train with pulse width limited by the bandwidth of the photodetector and sampling head (note the lessened negative ringing with the longer pulses as compared to Systems 1-3, indicating a true pulse width which is longer than those of those systems).

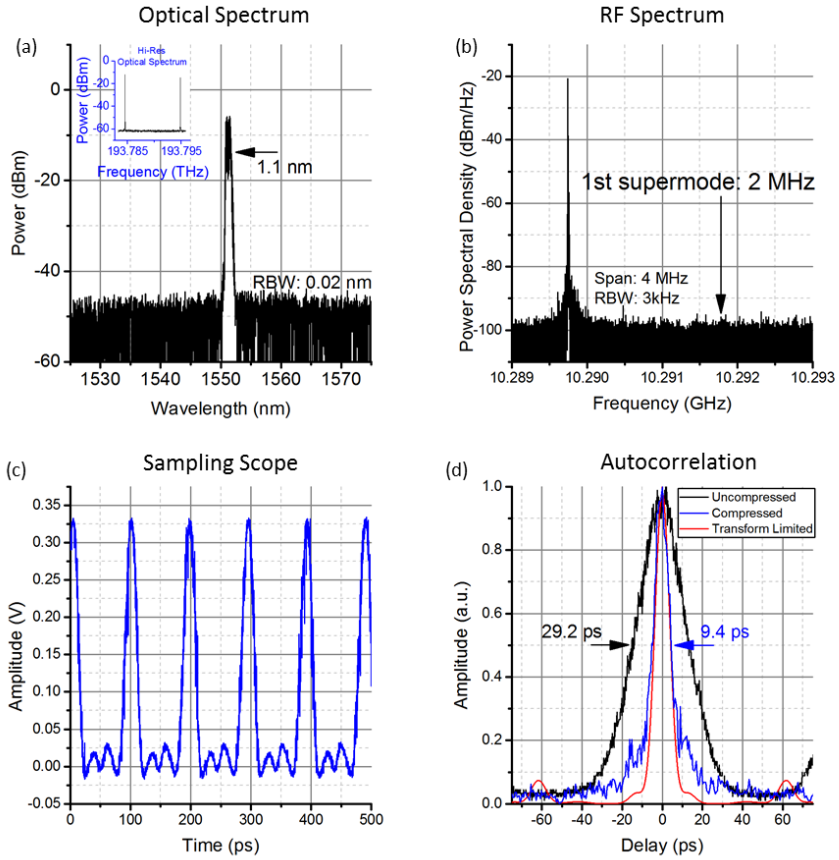

Figure 25 Optical and RF characterization data for System 4 (SCOWA, Long cavity, 10k finesse FPE). (a) Optical spectrum; (a, inset) Hi-res optical spectrum; (b) photodetected RF spectrum; (c) sampling scope trace of photodetected compressed pulses; (d) autocorrelation for uncompressed (black), compressed (blue) and transform-limited (red) pulses

Figure 26 shows the linewidth and long-term stability performance for System 4. The heterodyne beat note measurement was limited by the linewidth of the reference CW laser used (100 Hz). Predicted linewidth performance will be discussed more in the following section. The Allan deviation reaches a minimum of 4×10^{-12} at an averaging time of 30 ms.

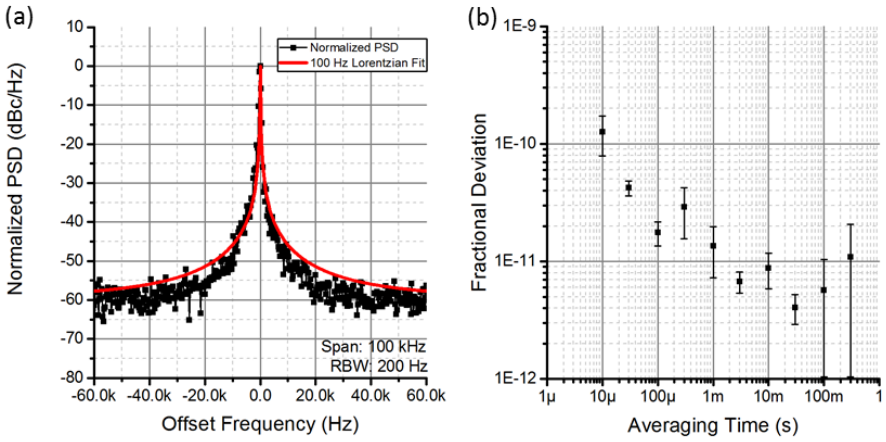

Figure 26 Linewidth and long term stability data for System 4 (SCOWA, long cavity, 10k finesse): (a) heterodyne beat with a 100-Hz reference CW laser. The beatnote center frequency was ~4 GHz. The measurement limit of a 100-Hz Lorentzian function with an added noise floor of -58 dBc/Hz (red) is shown for visual aid; (b) Allan deviation measurement of a heterodyne beat with a cavity-stabilized CW laser.

5.1.5 System 5: SCOWA, short cavity, 1000 finesse FPE

In addition to the four systems with a high finesse FPE, one system with an FPE of low finesse (10^3) was also measured for linewidth and Allan deviation performance. The system had a short cavity length and was SCOWA-based. This configuration has been reported on before for optical and RF characteristics in addition to phase noise performance [14]. Presented here in Figure 27 are linewidth and Allan deviation data to attempt to complete the set of performance data for the configuration. The heterodyne linewidth measurement follows a 300 Hz Lorentzian fit. The Allan deviation at low averaging times agrees with that of the corresponding high finesse FPE system, which fits with the hypothesis that stability at short averaging times is dominated by the stability of the mode-locking driving signal. However, for longer averaging times, this system's stability performance branches upwards. Although it was predicted that FPE finesse would influence stability at longer averaging times due to frequency selectivity of the resulting laser cavity, the increase seen here is more likely due to the conditions under which this iteration of the

configuration was constructed. The laser enclosure could not accommodate the large low finesse FPE assembly in addition to the other laser cavity elements. So as not to disturb the high finesse FPE assembly, fiber length was added and routed outside of the laser enclosure over a distance of about 1 meter to reach the etalon. This exposed about two meters of the laser cavity to the lab environment outside of the laser enclosure. In addition, the low finesse FPE assembly does not allow for a free-space polarization beam splitter to be inserted for the purposes of PDH light injection. The architecture was thus somewhat modified to use a fiber polarization beam splitter before the output coupler. It has been observed in the past that the fiber PBS has an extinction ratio which is about 10 dB worse than the free-space PBS. More importantly, any disturbance to the fiber between the etalon and the fiber PBS (where both laser and PDH light co-propagate) can cause undesired leakage between the laser and the PDH ports of the PBS. This has been seen to introduce some noise in laser performance, but the bigger effect is seen in the PDH error signal, and thus the stabilization performance, which shows up at longer averaging times in the Allan

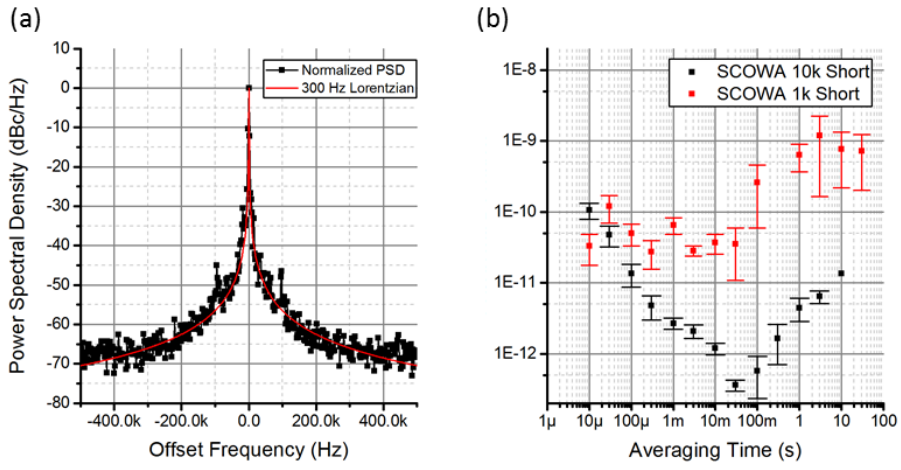

Figure 27 (a) heterodyne beat between a combline from System 5 and a 100-Hz CW reference laser. A 300 Hz Lorentzian function with an appropriate noise floor level is shown in red for visual aid; (b) Allan deviation measurements of a heterodyne beat with a cavity-stabilized CW laser, normalized to the optical frequency of 193.4 THz for both System 3 (black) and System 5 (red)

deviation measurement. Thus, it is probably not appropriate to make any statement on the Allan deviation performance of this system as compared to the other systems under study.

5.2 Discussion

5.2.1 Phase Noise of Photodetected Output

Although the long cavities were not able to be stabilized for long enough to acquire phase noise data, comparison between the SCOWA and SOA systems is still possible. Figure 28 shows the phase noise and integrated timing jitter for Systems 1 and 3 (10k finesse FPE, short cavity length, with SOA and SCOWA gain, respectively). There are a few points to make here. The most obvious one is the decrease in the shot noise floor as a result of the higher power incident on the photodetector for the SCOWA system.

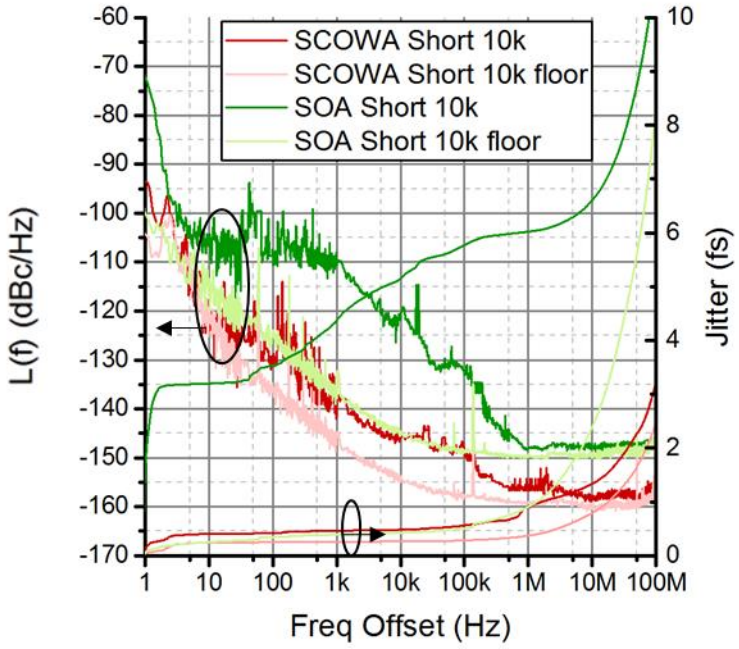

Figure 28 Single sideband residual phase noise measurement for Systems 1 (green) and 3 (red), with associated measurement noise floors (muted green, muted red, respectively).

In addition, the noise at low offset frequencies (<10 Hz) is dramatically reduced in the SCOWA case. This is to be expected given the improvement in optical mode linewidth from the increase in intracavity power.

Both cavities show a similar white noise plateau corner frequency near 100 kHz, as expected since they have the same cavity length. The fact that the level of the white noise plateau is lower by nearly 20 dB for the SCOWA-based system can be traced to the difference in peak power incident on the photodetector.

5.2.2 Long term Optical Frequency Stability

Compiled in Figure 29 are all of the Allan deviation data for the configurations with an FPE of finesse 10^4. There is no marked difference in behavior between the SCOWA and SOA configurations. On the other hand, cavity length shows a clear effect on stability at middling timescales. At short timescales (10-100 μs), the fractional frequency deviation is approximately the same for all configurations. Between averaging times of 100 μs and 100 ms, there is a splitting in performance between the long and short cavity configurations. This is also the frequency range (10 Hz – 10 kHz) at which phase noise is acquired due to propagation through long, unstabilized fiber lengths. Although the PDH length stabilization is in place to mitigate just such an effect, there may be some effect still visible in this sensitive measurement at these timescales due to the multipass nature of a laser cavity. This also provides a clue as to why the residual phase noise measurement was not feasible to perform for the long cavity cases. Because of the difficulty in

achieving a long term PDH lock for the long cavity cases, it is unclear whether the performance of the short and long cavity cases joins up again at longer timescales.

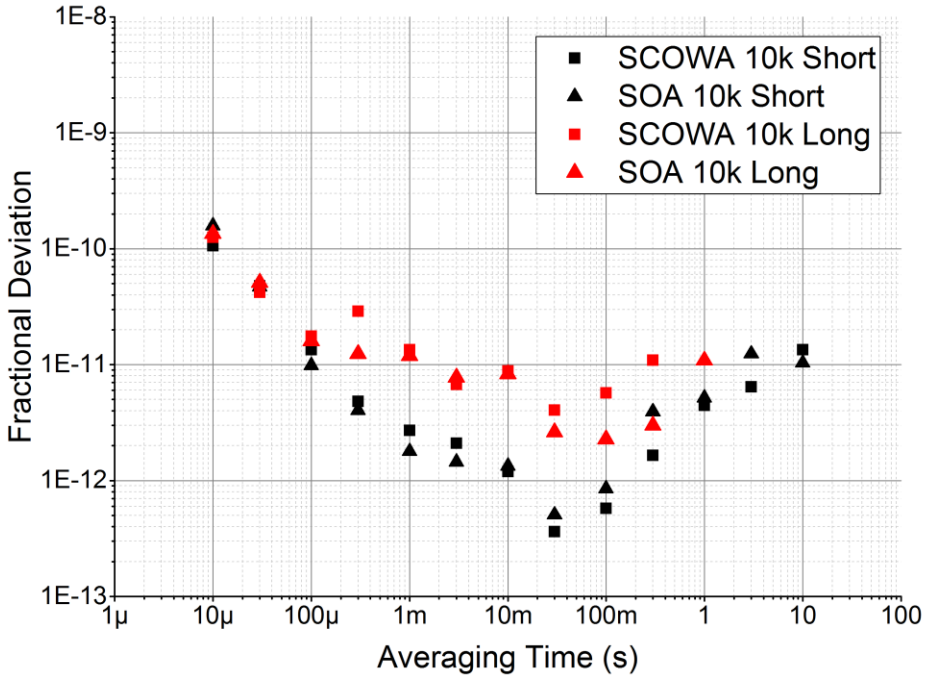

Figure 29 Allan deviation data for all configurations using an FPE of finesse 10^4. Long cavities (red) short cavities (black) SCOWA (square symbol) and SOA (triangle symbol)

5.2.3 Optical Mode Linewidth

The attempt at independent variation of intracavity power and passive cavity resonance width was ultimately unsuccessful, so care was taken when comparing the linewidth measurements across systems. A fair comparison of the optical mode linewidths of each system is performed by calculating the intracavity power, the passive cavity resonance width, and the combline linewidth.

Assuming that the reference CW laser and the combline being measured are both Lorentzian in lineshape, their heterodyne beat is also Lorentzian with a width equal to the sum of the widths of the two optical tones producing the beat. The reference CW laser used for these

measurements has a factory-specified linewidth of 100 Hz, so in comparing the linewidth performance, the actual optical mode linewidth will be 100 Hz less than the measured heterodyne beatnote linewidth. This presents a difficulty for directly analyzing System 4 especially, whose heterodyne beatnote width was already measurement-limited at a width of 100 Hz. However, given the trends observed across the remaining systems and the calculated passive cavity resonance width and intracavity power, System 4's linewidth performance can be predicted if not directly measured with this setup. Table 3 summarizes the linewidth performance of each system, as well as the individual system parameters which are used in calculating the passive cavity resonance width.

Table 3 Comparison of optical mode linewidths between the 5 systems (FPE Finesse = 10^4 unless otherwise indicated)

System	Intracavity Power (mW)	Cavity Length (m)	Measured Heterodyne Linewidth (Hz)	Assumed Optical Linewidth (Hz)
1. SOA Short	50	12.5	1.3k	1.2k
2. SOA Long	26	93.5	150	50
3. SCOWA Short	110	12.5	125	25
4. SCOWA Long	80	93.5	100	*
5. SOA Short (FPE Finesse = 1000)	34	15.5	300	200

Calling back to the modified Schawlow-Townes linewidth equation presented in Section 3.1.1, Table 4 enumerates the values used for the remaining variables in the modified S-T equation introduced in Section 3.1.1, with the addition of an added multiplier for technical noise in the lab environment. It is difficult to reach the S-T limit under normal operating conditions (at room temperature, open to the lab environment, line noise, etc.), but since all systems were operated

under similar conditions, a single factor which resulted in least error for Systems 1-3 and 5 was used.

Calculating the passive cavity resonance width requires knowledge of the cavity length and of the total parasitic losses of the system. Although care was taken to keep losses relatively constant across systems, some variation was ultimately observed to affect performance. Adding the fiber spool for long cavity systems added an additional 1.1 dB insertion loss to the cavity. In addition, the FPE assembly with finesse of 1000 has more loss than the FPE assembly with finesse of 10000 due to its more complex free-space coupling optics. Finally, the SOA used had some coupling losses due to more stringent polarization selectivity of this device waveguide compared to the SCOWA.

Table 4 Additional relevant parameters for linewidth comparison.

Parameter	**Value**
Optical frequency, ν (THz)	c/1550 nm = 193.4 THz
Spontaneous Emission Factor, θ	3
Linewidth Enhancement Factor, α	6.2
Experimental noise factor	30 dB
Parasitic loss (l_{tot}) for short cavity systems	14 dB
Parasitic loss (l_{tot}) for long cavity systems	15 dB
Additional loss for 1k finesse FPE assembly	5 dB
Additional parasitic loss for SOA gain-based system	6 dB

For visual analysis across systems, linewidth is plotted as a function of passive cavity resonance width. According to the modified S-T equation, for a given output power, linewidth varies quadratically with passive cavity resonance width.

Figure 30 shows this relationship for the systems studied here. For the plots in

Figure 30, the gray shaded region is included for visual aid and represents the linewidth curves which fall within a range of output powers between 2 and 12 mW. The dashed lines indicate the theoretical linewidth vs. resonance width curve for the output power corresponding to the systems in the plot, and all measured data points show good agreement with their theoretical linewidth curve.

Figure 30 (a) is the comparison of SOA cavities with short and long cavity round trip times. Although there was an additional insertion loss associated with adding the long fiber spool of 1.1 dB which causes an upward shift for its power curve, the decrease in passive cavity resonance width still resulted in a decrease in linewidth by more than one decade from 1.2 kHz to 50 Hz.

Figure 30 (b) is comparison of short cavity systems with SOA and SCOWA gain media. Here, the increase in output power and the decrease in passive cavity resonance width (due largely to lower loss fiber-to-chip coupling in the SCOWA device) result in a decrease in optical mode linewidth from 1.2 kHz to 25 Hz.

Figure 30 (c) shows the reduction in linewidth for the SCOWA short cavity system by swapping the 1000 finesse FPE for the 10000 finesse FPE. Although etalon finesse itself is not expected to influence linewidth performance, the lower insertion loss of the high finesse FPE assembly results in a decrease in parasitic loss of the system to both increase output power and reduce passive cavity resonance width. The insertion loss of the 1k finesse system was measured

to be 5 dB more than that of the 10k finesse assembly, and the system linewidth is reduced from 200 Hz to 25 Hz. Finally

Figure 30 (d) predicts performance of System 4 given that the model has been consistent with the other systems. Given the calculated passive cavity resonance width and the measured output power, the linewidth performance of the SCOWA long cavity system is expected to lie within a range of 0.5-1 Hz.

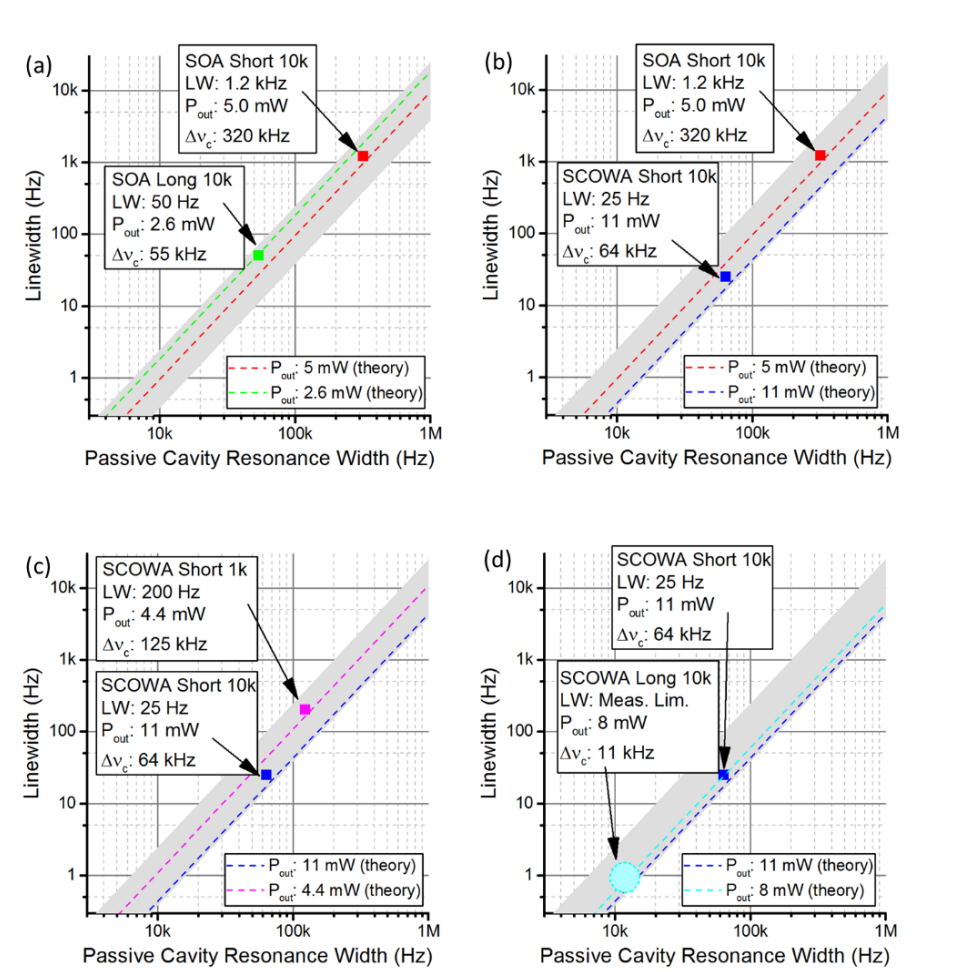

Figure 30 Selected comparisons in linewidth performance vs. passive cavity resonance width of nested cavity systems. Gray shaded region of each plot represents range of curves with output powers lying between 2 and 12 mW. Dotted lines are the specific linewidth curve determined by the power of the system under study (a) SOA, 10^4 finesse systems with short length (red) and long length (green); (b) Short, 10^4

finesse systems with SOA gain medium (red) and SCOWA gain medium (blue); (c) Short SCOWA systems with 10^3 finesse FPE (pink) and 10^4 finesse FPE (blue); (d) SCOWA, 10^4 finesse FPE systems with short length (blue), and the expected linewidth performance for long cavity length (light blue).

,

Figure 31 shows the summary of all measured system linewidths. It is worth noting that the relative decrease in linewidth by increasing the cavity length is predicted to be the same for both the SCOWA-based systems and the SOA-based systems, as indicated by the blue curved arrows.

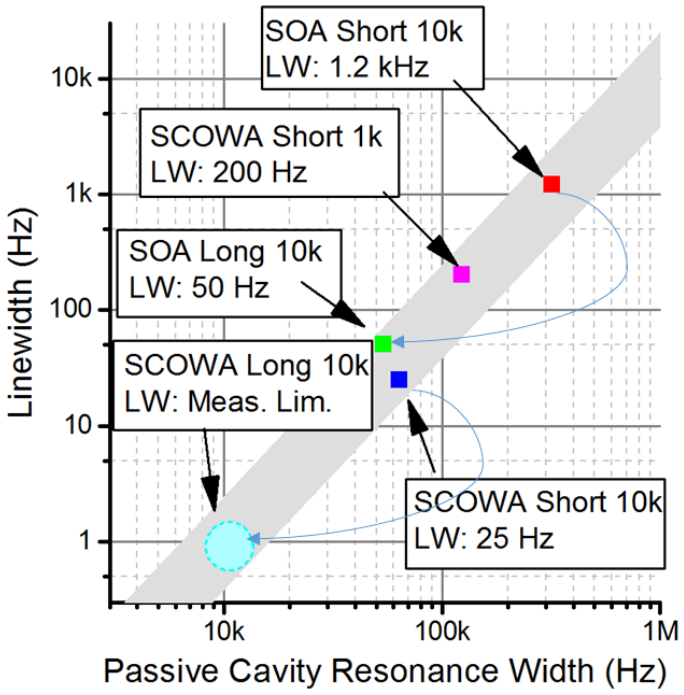

Figure 31 Compiled and annotated linewidth results. Gray shaded region: range of linewidth performance curves for systems with output powers between 2 and 12 mW. Agreeing with theory, linewidth decreases with longer cavity length, and increases with increased cavity losses. Also agreeing with theory, the relationship between the linewidth performance short and long configurations is the same for SCOWA-based and SOA-based systems

CHAPTER 6: SUMMARY AND OUTLOOK

The nested cavity architecture has been shown to perform well in several metrics for optical and RF performance. In this work alone, narrow linewidth, low timing jitter, and high frequency stability have been shown to occur from a single system. As these metrics are pushed to new limits by increasing the quality of elements in the laser cavity, it becomes clear that although the architecture is extremely flexible to fit the application, some trade-offs to performance occur. It was shown that adding cavity length in order to decrease passive resonance width is successful at decreasing optical mode linewidth, but makes nearly every other performance metric (power, frequency stability, phase noise, bandwidth, free-running stability) suffer. In addition, replacing the conventional SOA with the high saturation power gain SCOWA improved nearly all aspects of performance, but made the resulting system much more intolerant to loss and reliant on thermal management.

The future direction of the growth of this architecture can be somewhat directed by this work. The measurements presented here show that unless linewidth is prized at the expense of phase noise, bandwidth, etc., system performance may best be served by keeping the cavity length low. On the other hand, it may be desired to explore further stabilization in order to realize cavity length without sacrificing stability. A simple passive stabilization method which would greatly aid performance would be the simple substitution of polarization maintaining fiber for most of the standard SMF. This would eliminate instabilities caused by polarization drift. A more labor-intensive action to improve stability would be to revisit thermal management of the system. At present, only the gain medium and the FPE are thermally controlled. As cavity length is increased to 100s of meters, it may be helpful to provide thermal management for the laser enclosure itself.

The primary aim and result of this work was to shed light on the interplay of the cavity elements of this complex architecture. Even so, record-breaking results for the architecture were also measured. The third system in particular (SCOWA, short cavity, high finesse FPE) out-performed previous systems by two orders of magnitude for frequency stability (3×10^{-13} fractional deviation) and also had low timing jitter (23 fs integrated to Nyquist) and maintained narrow optical mode linewidth at 25 Hz FWHM. The fourth system (SCOWA, long cavity, high finesse FPE) had measurement-limited linewidths, and showed evidence of Hz-level linewidth performance. It is the hope of the author that this parametric study will enable strategic advancement of the performance of nested cavity systems.

REFERENCES

1. Diddams, S.A., et al., *Design and control of femtosecond lasers for optical clocks and the synthesis of low-noise optical and microwave signals.* IEEE Journal of Selected Topics in Quantum Electronics, 2003. **9**(4): p. 1072-1080.
2. Fortier, T.M., et al., *Generation of ultrastable microwaves via optical frequency division.* Nat Photon, 2011. **5**(7): p. 425-429.
3. DePriest, C.M., et al., *High-quality photonic sampling streams from a semiconductor diode ring laser.* Ieee Journal of Quantum Electronics, 2002. **38**(4): p. 380-389.
4. Mandridis, D., et al., *Low-noise, low repetition rate, semiconductor-based mode-locked laser source suitable for high bandwidth photonic analog-digital conversion.* Applied Optics, 2010. **49**(15): p. 2850-2857.
5. Piracha, M.U., et al., *Range resolved lidar for long distance ranging with sub-millimeter resolution.* Optics Express, 2010. **18**(7): p. 7184-7189.
6. Piracha, M.U., et al., *Simultaneous ranging and velocimetry of fast moving targets using oppositely chirped pulses from a mode-locked laser.* Optics Express, 2011. **19**(12): p. 11213-11219.
7. Coddington, I., et al., *Rapid and precise absolute distance measurements at long range.* Nature Photonics, 2009. **3**(6): p. 351-356.
8. Coddington, I., W.C. Swann, and N.R. Newbury, *Coherent multiheterodyne spectroscopy using stabilized optical frequency combs (vol 100, art no 013902, 2008).* Physical Review Letters, 2008. **101**(4).
9. Braje, D.A., et al., *Astronomical spectrograph calibration with broad-spectrum frequency combs.* European Physical Journal D, 2008. **48**(1): p. 57-66.
10. Papp, S.B., et al., *Microresonator frequency comb optical clock.* Optica, 2014. **1**(1): p. 10-14.
11. Quinlan, F., et al., *Ultralow-jitter and amplitude-noise semiconductor-based actively mode-locked laser.* Optics Letters, 2006. **31**(19): p. 2870-2872.
12. Gee, S., et al., *Simultaneous optical comb frequency stabilization and super-mode noise suppression of harmonically mode-locked semiconductor ring laser using an intracavity etalon.* Ieee Photonics Technology Letters, 2005. **17**(1): p. 199-201.
13. Gee, S., et al., *Ultralow-noise mode-locked optical pulse trains from an external cavity laser based on a slab coupled optical waveguide amplifier (SCOWA).* Optics Letters, 2005. **30**(20): p. 2742-2744.

14. Davila-Rodriguez, J., et al., *Ultralow Noise, Etalon Stabilized, 10-GHz Optical Frequency Comb Based on an SCOW Amplifier.* Ieee Photonics Technology Letters, 2012. **24**(23): p. 2159-2162.
15. Yilmaz, T., et al., *Measurement of residual phase noise and longitudinal-mode linewidth in a hybridly mode-locked external linear cavity semiconductor laser.* Optics Letters, 2002. **27**(10): p. 872-874.
16. Bartels, A., D. Heinecke, and S.A. Diddams, *Passively mode-locked 10 GHz femtosecond Ti:sapphire laser.* Optics Letters, 2008. **33**(16): p. 1905-1907.
17. Fortier, T.M., A. Bartels, and S.A. Diddams, *Octave-spanning Ti:sapphire laser with a repetition rate >1 GHz for optical frequency measurements and comparisons.* Optics Letters, 2006. **31**(7): p. 1011-1013.
18. Savchenkov, A.A., et al., *Tunable Optical Frequency Comb with a Crystalline Whispering Gallery Mode Resonator.* Physical Review Letters, 2008. **101**(9): p. 093902.
19. Hartl, I., et al. *Fully Stabilized GHz Yb-Fiber Laser Frequency Comb*. in *Advanced Solid-State Photonics*. 2009. Denver, Colorado: Optical Society of America.
20. Schibli, T.R., et al., *Optical frequency comb with submillihertz linewidth and more than 10 W average power.* Nature Photonics, 2008. **2**(6): p. 355-359.
21. Akbulut, M., et al., *Measurement of carrier envelope offset frequency for a 10 GHz etalon-stabilized semiconductor optical frequency comb.* Optics Express, 2011. **19**(18): p. 16851-16865.
22. Brabec, T., et al., *Kerr lens mode locking.* Optics Letters, 1992. **17**(18): p. 1292-1294.
23. Haus, H.A., *Theory of mode locking with a fast saturable absorber.* Journal of Applied Physics, 1975. **46**(7): p. 3049-3058.
24. Haus, H. and P.-T. Ho, *Effect of noise on active mode locking of a diode laser.* IEEE Journal of Quantum Electronics, 1979. **15**(11): p. 1258-1265.
25. Kuizenga, D. and A. Siegman, *FM and AM mode locking of the homogeneous laser-Part I: Theory.* IEEE Journal of Quantum Electronics, 1970. **6**(11): p. 694-708.
26. Delfyett, P., et al., *Femtosecond hybrid mode-locked semiconductor laser and amplifier dynamics.* Applied Physics B: Lasers and Optics, 1994. **58**(3): p. 183-195.
27. Quinlan, F., et al., *Harmonically mode-locked semiconductor-based lasers as high repetition rate ultralow noise pulse train and optical frequency comb sources.* Journal of Optics a-Pure and Applied Optics, 2009. **11**(10).

28. Davila-Rodriguez, J., et al., *A semiconductor-based, frequency-stabilized mode-locked laser using a phase modulator and an intracavity etalon.* Optics Letters, 2010. **35**(24): p. 4130-4132.
29. Davila-Rodriguez, J., K. Bagnell, and P.J. Delfyett, *Frequency stability of a 10 GHz optical frequency comb from a semiconductor-based mode-locked laser with an intracavity 10,000 finesse etalon.* Optics Letters, 2013. **38**(18): p. 3665-3668.
30. Klee, A., K. Bagnell, and P. Delfyett. *Stabilized Semiconductor Optical Frequency Comb with Programmable Intracavity Dispersion Compensation*. in *Frontiers in Optics 2014*. 2014. Tucson, Arizona: Optical Society of America.
31. Yablonovitch, E. and E. Kane, *Band structure engineering of semiconductor lasers for optical communications.* Journal of lightwave technology, 1988. **6**(8): p. 1292-1299.
32. Becker, M., D. Kuizenga, and A. Siegman, *Harmonic mode locking of the Nd:YAG laser.* IEEE Journal of Quantum Electronics, 1972. **8**(8): p. 687-693.
33. Bagnell, K., A. Klee, and P. Delfyett. *Study of White Noise Corner Frequency Location in Residual Phase Noise Measurement with Short and Long Cavity Lengths*. in *Frontiers in Optics 2015*. 2015. San Jose, California: Optical Society of America.
34. Williams, C., *Stabilization of an Injection Locked Harmonically Mode-Locked Laser via Polarization Spectroscopy for Frequency Comb Generation.* CLEO 2012, 2012.
35. Williams, C., F. Quinlan, and P.J. Delfyett, *Injection-Locked Mode-Locked Laser With Long-Term Stabilization and High Power-per-Combline.* Ieee Photonics Technology Letters, 2009. **21**(1-4): p. 94-96.
36. Li, Y., et al., *Novel method to simultaneously compress pulses and suppress supermode noise in actively mode-locked fiber ring laser.* IEEE Photonics Technology Letters, 1998. **10**(9): p. 1250-1252.
37. Gee, S., et al., *Self-stabilization of an actively mode-locked semiconductor-based fiber-ring laser for ultralow jitter.* Ieee Photonics Technology Letters, 2007. **19**(5-8): p. 498-500.
38. Drever, R.W.P., et al., *Laser Phase and Frequency Stabilization Using an Optical-Resonator.* Applied Physics B-Photophysics and Laser Chemistry, 1983. **31**(2): p. 97-105.
39. Black, E.D., *An introduction to Pound-Drever-Hall laser frequency stabilization.* American Journal of Physics, 2001. **69**(1): p. 79-87.

40. Ozdur, I., et al., *Modified Pound-Drever-Hall scheme for high-precision free spectral range measurement of Fabry-Perot etalon.* Electronics Letters, 2008. **44**(15): p. 927-929.
41. Ozdur, I., et al., *A Semiconductor-Based 10-GHz Optical Comb Source With Sub 3-fs Shot-Noise-Limited Timing Jitter and similar to 500-Hz Comb Linewidth.* Ieee Photonics Technology Letters, 2010. **22**(6): p. 431-433.
42. Bagnell, K., A. Klee, and P. Delfyett. *A 10-GHz Optical Frequency Comb from a SCOWA-Based Mode-Locked Laser with 600-Hz Optical Mode Linewidth*. in *Frontiers in Optics 2016*. 2016. Rochester, New York: Optical Society of America.
43. Schawlow, A.L. and C.H. Townes, *Infrared and Optical Masers.* Physical Review, 1958. **112**(6): p. 1940-1949.
44. Lax, M., *Classical Noise. V. Noise in Self-Sustained Oscillators.* Physical Review, 1967. **160**(2): p. 290-307.
45. Rush, D., G. Burdge, and P.-T. Ho, *The linewidth of a mode-locked semiconductor laser caused by spontaneous emission: experimental comparison to single-mode operation.* IEEE journal of quantum electronics, 1986. **22**(11): p. 2088-2091.
46. Ho, P.T., *Phase and amplitude fluctuations in a mode-locked laser.* IEEE Journal of Quantum Electronics, 1985. **21**(11): p. 1806-1813.
47. Henry, C., *Theory of the linewidth of semiconductor lasers.* IEEE Journal of Quantum Electronics, 1982. **18**(2): p. 259-264.
48. Henry, C., *Theory of spontaneous emission noise in open resonators and its application to lasers and optical amplifiers.* Journal of lightwave technology, 1986. **4**(3): p. 288-297.
49. Osinski, M. and J. Buus, *Linewidth broadening factor in semiconductor lasers--An overview.* IEEE Journal of Quantum Electronics, 1987. **23**(1): p. 9-29.
50. Allan, D.W., *Statistics of Atomic Frequency Standards.* Proceedings of the Institute of Electrical and Electronics Engineers, 1966. **54**(2): p. 221-&.
51. Allan, D.W., *Time and Frequency (Time-Domain) Characterization, Estimation, and Prediction of Precision Clocks and Oscillators.* Ieee Transactions on Ultrasonics Ferroelectrics and Frequency Control, 1987. **34**(6): p. 647-654.
52. Quinlan, F., et al., *The effects of filtering RF source phase noise by a low noise, high quality factor actively modelocked laser on the laser's absolute and relative phase noise.* Optics Express, 2006. **14**(12): p. 5346-5355.

53. Juodawlkis, P.W., et al., *High-power 1.5-μm InGaAsP-InP slab-coupled optical waveguide amplifier*. IEEE Photonics Technology Letters, 2005. **17**(2): p. 279-281.